ORAU TEAM
Dose Reconstruction
Project for NIOSH

Oak Ridge Associated Universities | Dade Moeller | MJW Technical Services

Correction Factors for Use with ICRP Publication 116 Isotropic and Rotational Dose Conversion Coefficients	ORAUT-RPRT-0068	Rev. 00
	Effective Date:	07/11/2016
	Supersedes:	None

Subject Expert(s): Richard J. Traub, Matthew H. Smith, Keith A. McCartney

Document Owner Approval:	Signature on File Matthew H. Smith, Document Owner	Approval Date:	06/03/2016
Concurrence:	Signature on File John M. Byrne, Objective 1 Manager	Concurrence Date:	06/02/2016
Concurrence:	Signature on File Edward F. Maher, Objective 3 Manager	Concurrence Date:	06/02/2016
Concurrence:	Dianne Poncio Signature on File for Kate Kimpan, Project Director	Concurrence Date:	06/06/2016
Approval:	Signature on File James W. Neton, Associate Director for Science	Approval Date:	07/11/2016

FOR DOCUMENTS MARKED AS A TOTAL REWRITE, REVISION, OR PAGE CHANGE, REPLACE THE PRIOR REVISION AND DISCARD / DESTROY ALL COPIES OF THE PRIOR REVISION.

☒ New ☐ Total Rewrite ☐ Revision ☐ Page Change

PUBLICATION RECORD

EFFECTIVE DATE	REVISION NUMBER	DESCRIPTION
07/11/2016	00	New document initiated for evaluation of correction factors for use with ICRP Publication 116 rotational dose conversion coefficients and for neutron irradiations which includes information for use with ICRP Publication 110 isotropic dose conversion coefficients. Incorporates formal internal and NIOSH review comments. Training required: As determined by the Objective Manager. Initiated by Matthew H. Smith.

TRADEMARK INFORMATION

TABLE OF CONTENTS

SECTION **TITLE** **PAGE**

Acronyms and Abbreviations 6

1.0 Introduction 7

2.0 Methods and Approach 7
2.1 Phantoms 8
2.2 Dosimeters 9
2.3 Calculations 9
2.4 Benchmark Calculations 9
2.5 Irradiation Geometry Factors 9

3.0 Results 10
3.1 Benchmark calculations 10
3.2 Irradiation Geometry Factors 10
3.2.1 Photon Irradiations 10
3.2.2 Neutron Irradiations 13
3.3 Angular Response 16

4.0 Discussion 17

5.0 Summary 18

References 19

ATTACHMENT A DOSIMETER LOCATIONS ON THE ADULT FEMALE VOXEL PHANTOM 20
ATTACHMENT B DOSIMETER LOCATIONS ON THE ADULT MALE VOXEL PHANTOM 27
ATTACHMENT C EXAMPLE MCNP6 INPUT FILE 32
ATTACHMENT D RESULTS OF REFERENCE CALCULATIONS 54

LIST OF TABLES

TABLE **TITLE** **PAGE**

2-1 Dimensions of the ICRP Publication 110 voxel phantoms 8
2-2 Dosimeter locations 9
3-1 Estimated ROT IGFs for monoenergetic photons incident on a voxel phantom 13
3-2 Estimated ISO IGFs for monoenergetic photons incident on a voxel phantom 13
3-3 Estimated ROT IGFs for monoenergetic neutrons incident on a voxel phantom 16
3-4 Estimated ISO IGFs for monoenergetic neutrons incident on a voxel phantom 16

LIST OF FIGURES

FIGURE **TITLE** **PAGE**

3-1 IGFs for uncollided photons in dosimeter regions when the adult female voxel phantom is irradiated in the ROT geometry by monoenergetic photons ... 11
3-2 IGFs for uncollided photons in dosimeter regions when the adult female voxel phantom is irradiated in the ISO geometry by monoenergetic photons ... 11
3-3 IGFs for uncollided photons in dosimeter regions when the adult male voxel phantom is irradiated in the ROT geometry by monoenergetic photons. ... 12
3-4 IGFs for uncollided photons in dosimeter regions when the adult male voxel phantom is irradiated in the ISO geometry by monoenergetic photons ... 12
3-5 IGFs for uncollided neutrons in dosimeter regions when the adult female voxel phantom is irradiated in the ROT geometry by monoenergetic neutrons ... 14
3-6 IGFs for uncollided neutrons in dosimeter regions when the adult female voxel phantom is irradiated in the ISO geometry by monoenergetic neutrons ... 14
3-7 IGFs for uncollided neutrons in dosimeter regions when the adult male voxel phantom is irradiated in the ROT geometry by monoenergetic neutrons ... 15
3-8 IGFs for uncollided neutrons in dosimeter regions when the adult male voxel phantom is irradiated in the ISO geometry by monoenergetic neutrons ... 15
3-9 Rotational dependence of fluence at four dosimeter locations for uncollided 0.2-MeV photons ... 17
A-1 Elevation view of the adult female voxel phantom showing the center chest dosimeter location ... 21
A-2 Plan view of the adult female voxel phantom showing the center chest dosimeter location ... 22
A-3 Elevation view of the adult female voxel phantom showing the left collar dosimeter location ... 22
A-4 Plan view of the adult female voxel phantom showing the left collar dosimeter location ... 23
A-5 Elevation view of the adult female voxel phantom showing the center waist dosimeter location ... 23
A-6 Plan view of the adult female voxel phantom showing the center waist dosimeter location ... 24
A-7 Elevation view of the adult female voxel phantom showing the left chest pocket dosimeter location ... 25
A-8 Plan view of the adult female voxel phantom showing the left chest pocket dosimeter location ... 26
B-1 Elevation view of the adult male voxel phantom showing the center chest and center waist dosimeter locations ... 28
B-2 Plan view of the adult male voxel phantom showing the center chest and left chest pocket dosimeter locations ... 29
B-3 Plan view of the adult male voxel phantom showing the center waist dosimeter location ... 29
B-4 Plan view of adult male voxel phantom showing the left collar dosimeter ... 30
B-5 Elevation view of the adult male voxel phantom showing the left collar dosimeter location. ... 30
B-6 Elevation view of the adult male voxel phantom showing the left chest pocket dosimeter location ... 31
D-1 Relative differences between ICRP-evaluated DCCs and ORAU Team-calculated DCCs, adult female reference organs, monoenergetic neutrons, AP geometry ... 57
D-2 Relative differences between ICRP-evaluated DCCs and ORAU Team-calculated DCCs, adult male reference organs, monoenergetic neutrons, AP geometry ... 57
D-3 Relative differences between ICRP-evaluated DCCs and ORAU Team-calculated DCCs, adult female reference organs, monoenergetic neutrons, ROT geometry. ... 58
D-4 Relative differences between ICRP-evaluated DCCs and ORAU Team-calculated DCCs, adult male reference organs, monoenergetic neutrons, ROT geometry. ... 58

D-5 Relative differences between ICRP-evaluated DCCs and ORAU Team-calculated DCCs, adult female reference organs, monoenergetic neutrons, ISO geometry 59
D-6 Relative differences between ICRP-evaluated DCCs and ORAU Team-calculated DCCs, adult male reference organs, monoenergetic neutrons, ISO geometry 59
D-7 Relative differences between ICRP-evaluated DCCs and ORAU Team-calculated DCCs, adult female reference organs, monoenergetic photons, AP geometry.................................. 60
D-8 Relative differences between ICRP-evaluated DCCs and ORAU Team-calculated DCCs, adult male reference organs, monoenergetic photons, AP geometry 60
D-9 Relative differences between ICRP-evaluated DCCs and ORAU Team-calculated DCCs, adult female reference organs, monoenergetic photons, ROT geometry................................ 61
D-10 Relative differences between ICRP-evaluated DCCs and ORAU Team-calculated DCCs, adult male reference organs, monoenergetic photons, ROT geometry.................................. 61
D-11 Relative differences between ICRP-evaluated DCCs and ORAU Team-calculated DCCs, adult female reference organs, monoenergetic photons, ISO geometry 62
D-12 Relative differences between ICRP-evaluated DCCs and ORAU Team-calculated DCCs, adult male reference organs, monoenergetic photons, ISO geometry 62
D-13 Comparison between ICRP-evaluated DCCs and ORAU Team-calculated DCCs, adult female and male urinary bladder wall, monoenergetic neutrons, AP geometry....................... 63

ACRONYMS AND ABBREVIATIONS

AP	anterior-posterior
cm	centimeter
DCC	dose conversion coefficient
DOE	U.S. Department of Energy
H(10)*	ambient deep dose equivalent
Hp(10)	personal deep dose equivalent
ICRP	International Commission on Radiological Protection
IGF	irradiation geometry factor
IREP	Interactive RadioEpidemiological Program
ISO	isotropic
keV	kiloelectron-volt, 1,000 electron-volts
MCNP	Monte Carlo n-particle
MeV	megaelectron-volt, 1 million electron-volts
mm	millimeter
NIOSH	National Institute for Occupational Safety and Health
ORAU	Oak Ridge Associated Universities
PA	posterior-anterior
pSv	picosievert
ROT	rotational
SRDB Ref ID	Site Research Database Reference Identification (number)

1.0 INTRODUCTION

The purpose of this report is to provide guidance on the application of the organ dose conversion coefficients (DCCs) from International Commission on Radiological Protection (ICRP) Publication 116, *Conversion Coefficients for Radiological Protection Quantities for External Radiation Exposures* (ICRP 2010). The DCCs in Publication 116 assume that the radiation beam is perpendicular (incident angle = 0) in relation to the personal deep dose equivalent [*Hp(10)*], ambient deep dose equivalent [*H*(10)*], and exposure measurements using either film badge or thermoluminescent dosimetry. While this assumption is reasonable and appropriate for the anterior-posterior (AP) exposure geometry, it could lead to an underestimate of the organ dose if appropriate irradiation geometry factors (IGFs) are not applied.

In a review conducted after a comment concern from the Advisory Board on Radiation and Worker Health (SC&A 2005), the National Institute for Occupational Safety and Health (NIOSH) determined that the rotational (ROT) and isotropic (ISO) DCCs as applied in OCAS-IG-001, *External Dose Reconstruction Implementation Guideline* (NIOSH 2007), could in fact lead to an underestimate of the external dose. The ISO geometry is of minor concern from a dose reconstruction standpoint because it is typically applied to the onsite ambient dose in which a person was not present during the measurement to effectively shield the dosimeter from low (<30 keV) and intermediate (30 to 250 keV) energy photons. However, if the ISO DCCs were applied to personal dosimeter measurements, they could result in an underestimate of the organ dose. Correction factors for ROT and ISO DCCs [applicable to the bone (red marrow and surface), esophagus, and lung] were published in Table 4.1.a of OCAS-IG-001, *External Dose Reconstruction Implementation Guideline* (NIOSH 2007), based on information in *Study of a Selection of 10 Historical Types of Dosemeter: Variation of the Response to Hp(10) with Photon Energy and Geometry of Exposure* (Thierry-Chef et al. 2002).

This report addresses the potential underestimate associated with the ROT and ISO DCCs for photons and neutrons and provides a method for determining irradiation geometry correction factors (IGFs) based on Monte Carlo n-particle (MCNP) modeling of dosimeter response associated with placement on realistic phantoms as described in ICRP Publication 110, *Adult Reference Computational Phantoms* (ICRP 2009).

2.0 METHODS AND APPROACH

All calculations were performed using MCNP6 Version 1.0 (Pelowitz 2013). MCNP6.1 is a general purpose Monte Carlo radiation transport code. MCNP6.1 was chosen for these calculations because it is the only version of MCNP that the Los Alamos National Laboratory will continue to support in the future. Three irradiation geometries were considered for this report: AP, ROT, and ISO.

The AP geometry is defined by ICRP to be when the ionizing radiation is incident on the front of the body in a direction orthogonal to its long axis (ICRP 2010). To simulate an AP geometry for the irradiation of the phantoms, a single plane source (60×200 cm^2) was placed directly in front of the voxel phantom and the radiation particles were directed from the source to the voxel phantom.

The ROT geometry is defined to be when the body is irradiated by a parallel beam of ionizing radiation, which rotates at a uniform rate around the long axis from a direction orthogonal to the long axis of the body (ICRP 2010). To simulate a ROT geometry for irradiation of the phantoms, a single plane source (60×200 cm^2) was rotated at 5-degree intervals around the phantom. In the 0-degree rotation, the radiation particles are incident on the front of the body in a direction orthogonal to its long axis, and is the same as the AP geometry. The plane source was rotated around the voxel phantom via the TR card (a “card” is a set of data or instructions for input to MCNP; TR indicates surface coordinate transformation). Seventy-two TR cards were implemented in a single MCNP6 input file; the appropriate TR card for a particular history was determined by the SDEF card (SDEF indicates source definition). In the 180-degree rotation, which is equivalent to the posterior-anterior (PA) geometry, the photons are incident on the back of the body in a direction orthogonal to its long axis. The 90-degree ROT geometry is equivalent to the left lateral geometry, and the 270-degree rotation is equivalent to the right lateral geometry.

The ISO geometry is defined by ICRP (2010) as being a radiation field in which the particle fluence per solid angle is independent of direction and location in space (ICRP 2010). To simulate an ISO geometry for irradiation of the phantoms, a single plane source (60 × 200 cm^2) was rotated around the phantoms such that the plane source was tangential to a uniformly located point on a sphere whose center was located at the approximate center of the voxel phantom. The coordinates of uniformly distributed points on the sphere were calculated using a Fibonacci grid function. Fibonacci grids were used because the points so chosen are very evenly distributed over the surface of the sphere (Hannay and Nye 2004; González 2009; Swinbank and Purser 2006). The source plane was rotated around the phantom via the TR card; the rotation matrix of the TR card was a function of the location of the point. One hundred TR cards were implemented in a single MCNP6 input file; the appropriate TR card for a particular history was determined by the SDEF card. Three independent sets of TR cards were prepared and run so that the ISO data in this report are based on 300 uniformly distributed points.

In agreement with Publication 116 (ICRP 2010), the radiation source and voxel phantom were placed in a vacuum.

2.1 PHANTOMS

For these calculations, the adult female and adult male computational voxel phantoms, described in Publication 110 (ICRP 2009), were each implemented in MCNP6 (Pelowitz 2013) as a type 1 lattice.

A voxel phantom is a three-dimensional object that consists of a large number of voxels. Each voxel in a given phantom is the same size (see Table 2-1). The position, chemical composition, and density of each voxel are not explicitly encoded in a phantom. However, the position of a voxel is inferred based on its position relative to the other voxels in the phantom. The elemental composition and density of a voxel is inferred from a single digit that represents the tissue type of that voxel. Thus, a file that contains a voxel phantom consists of a large number of integers, where each integer is the index number of a tissue type. In the ICRP phantoms, the file consists of integers that range from 0 to 141. The zero (0) tissue type is a void, or air that surrounds the actual phantom. When implemented in MCNP6, the tissue type is interpreted as a universe that fills a lattice. Because universe number zero is defined as the highest level universe, it was necessary to renumber all zeros to something else. For the NIOSH Project, all zeros were converted to 256. The size of the individual voxel is encoded in the MCNP6 input file. The voxel dimensions of the two phantoms are shown in Table 2-1. Note that the two phantoms have different voxel dimensions and the number of voxels in the adult female phantom is approximately twice that of the adult male phantom. The ICRP phantom distribution files also contain tabs that were removed from the file.

Table 2-1. Dimensions of the ICRP Publication 110 voxel phantoms.

Dimension	Adult female phantom[a]	Adult male phantom[a]
Rows	137	127
Columns	299	254
Slices	348	222
Volume	1.775 × 1.775 × 4.84 mm^3	2.137 × 2.137 × 8.0 mm^3

a. The voxel phantoms are type 1 lattices.

The phantom files were also converted to a compact form that used the "*n*R" feature for horizontal data to reduce the size of the input file and to allow MCNP6 to read the adult female phantom file. It had been observed that MCNPX, a version of MCNP that preceded MCNP6, would display error messages if a phantom of a certain number of voxels was presented to MCNPX and its Visual Editor (Vised) in the standard horizontal data card format.

2.2 DOSIMETERS

Four dosimeter locations were implemented for the calculations. The dosimeter location is an empty (void) rectangular parallelepiped 5.08 × 5.08 × 0.2 cm^3 in size. The locations are center chest, left collar, center waist, and left chest pocket. These locations were taken to approximate the standard locations of the dosimeters on a worker (see Table 2-2). Two-dimensional drawings that show the location of the dosimeters on the adult female and adult male phantoms are provided in Attachments A and B, respectively. An example MCNP6 input file is provided in Attachment C.

Table 2-2. Dosimeter locations.

Dosimeter location	Description
Center chest	The lower edge of the dosimeter location approximates the bottom of the phantom sternum.
Left collar	The upper edge of the dosimeter location approximates the top of the left clavicle.
Center waist	The dosimeter location is centered at the approximate location of the belt buckle.
Left chest pocket	The upper edge of the dosimeter approximates the location of the top edge of the left chest pocket of a laboratory coat.

2.3 CALCULATIONS

Two types of tallies were collected for these calculations. The first type, called an f4 tally, provides a track length estimate of the cell fluence. The second type, an f6 tally, is a track length estimate of cell fluence modified by an energy deposition (heating) function.

Calculations were performed for neutron and photon radiations.

2.4 BENCHMARK CALCULATIONS

The f6 tallies were used to calculate the doses to eight organs – the brain, heart wall, liver, lung, kidney, pancreas, thyroid, and urinary bladder wall – as a means of checking the implementations of the voxel phantoms and irradiation geometries. The ICRP-evaluated DCCs for fluence to dose for these eight organs (ICRP 2010) were visually compared with the corresponding DCCs that were calculated using MCNP6.1 for this report.

2.5 IRRADIATION GEOMETRY FACTORS

The dosimeter dose calculations used the f4 type tally that was modified to convert photon fluence (cm^{-2}) to *Hp(10)* in picosievert. For photons, the fluence to *Hp(10)* DCCs were the product of the fluence to air kerma factors in Table A.1 of ICRP Publication 74 (ICRP 1996) and the air kerma to *Hp(10)* factors in Table A.24 of Publication 74 (ICRP 1996). The *Hp(10)* picosievert values were collected in 1-keV energy intervals. For neutrons, the fluence to *Hp(10)* DCCs were those published in Table A.42 of Publication 74 (ICRP 1996).

The IGFs in this report are the quotient of the *Hp(10)* for AP irradiations divided by the *Hp(10)* for the ROT or ISO irradiation geometry, as appropriate.

3.0 RESULTS

3.1 BENCHMARK CALCULATIONS

Pointwise estimates of the relative difference between the ICRP-evaluated (2010) conversion coefficients for fluence to dose and those calculated for this report are shown in Attachment D. Visually, the DCCs calculated for this report appear to agree well with the ICRP (2010) DCCs. In particular, the plots of the ISO geometry appear to show overall agreements that are similar to the agreements shown for the AP and ROT irradiation geometries.

3.2 IRRADIATION GEOMETRY FACTORS

A dosimeter placed in any of the four locations described in this report will underestimate the *Hp(10)* to a worker who is actually being irradiated in a ROT or ISO geometry if the dosimeter was calibrated for an AP irradiation. This is because the dosimeter is shielded to varying degrees by the body during both ROT and ISO geometry irradiation.

The IGFs are based solely on the incident energy of the particle. The IGFs in this report are the quotient of the particle fluence in the dosimeter cell for AP irradiations divided by the particle fluence in the dosimeter cell for the ROT or ISO irradiation geometry, as appropriate. Because the *Hp(10)* and exposure values are the products of the fluence and appropriate conversion factors (ICRP 1987), IGFs based on the fluence are applicable for both *Hp(10)* and exposure calculations.

3.2.1 PHOTON IRRADIATIONS

Pointwise estimates of the IGFs for photons are shown in Figures 3-1 through 3-4. In the figures, the dotted vertical lines show the boundaries of the Interactive RadioEpidemiological Program (IREP) dose groupings.

The IGF factors for photons that irradiated the voxel phantoms in the ROT irradiation geometry, averaged over the IREP energy regions, are listed in Table 3-1. The IGF factors for photons that irradiated the voxel phantoms in the ISO irradiation geometry, averaged over the IREP energy regions, are listed in Table 3-2.

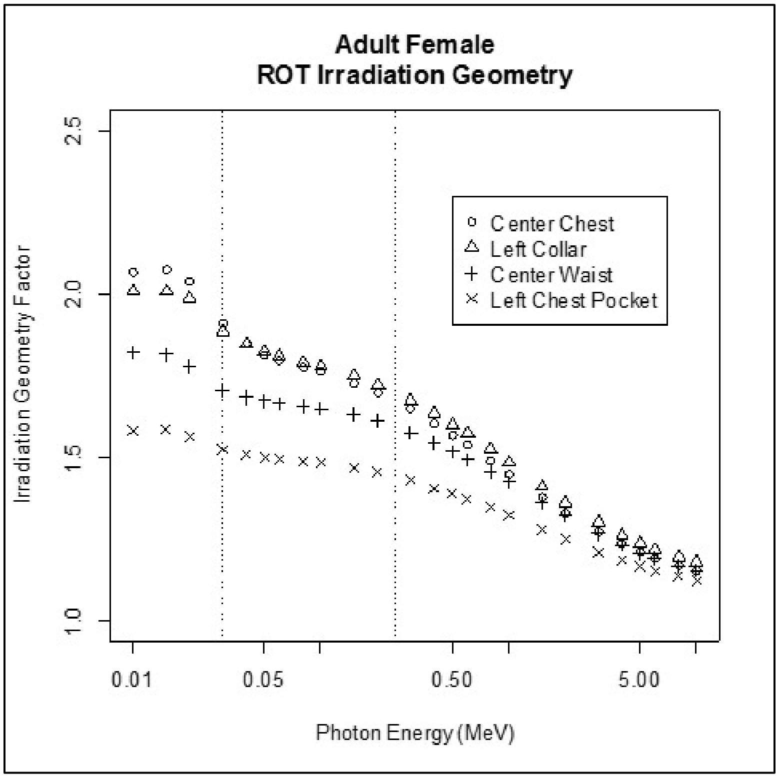

Figure 3-1. IGFs for uncollided photons in dosimeter regions when the adult female voxel phantom is irradiated in the ROT geometry by monoenergetic photons.

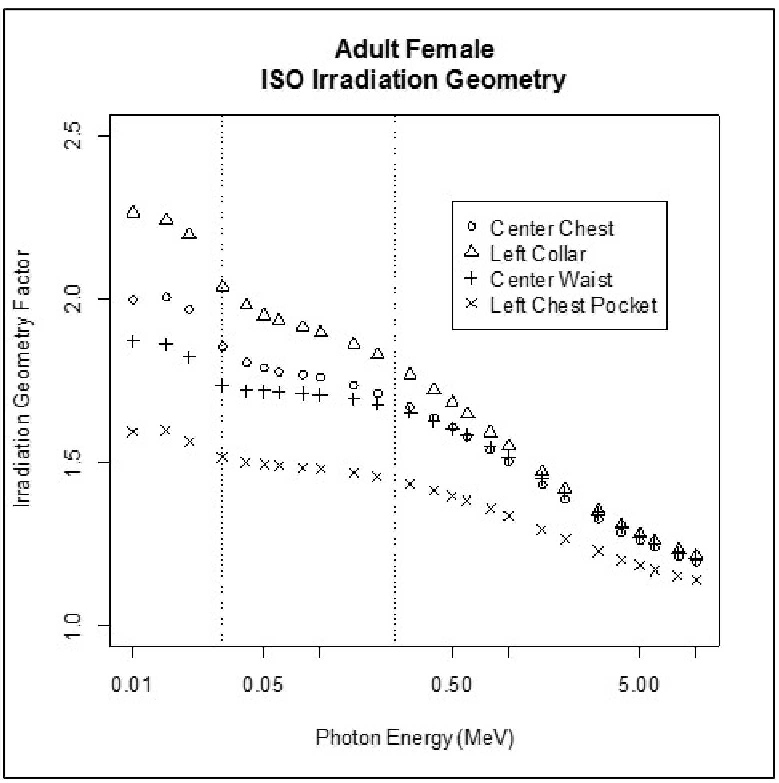

Figure 3-2. IGFs for uncollided photons in dosimeter regions when the adult female voxel phantom is irradiated in the ISO geometry by monoenergetic photons.

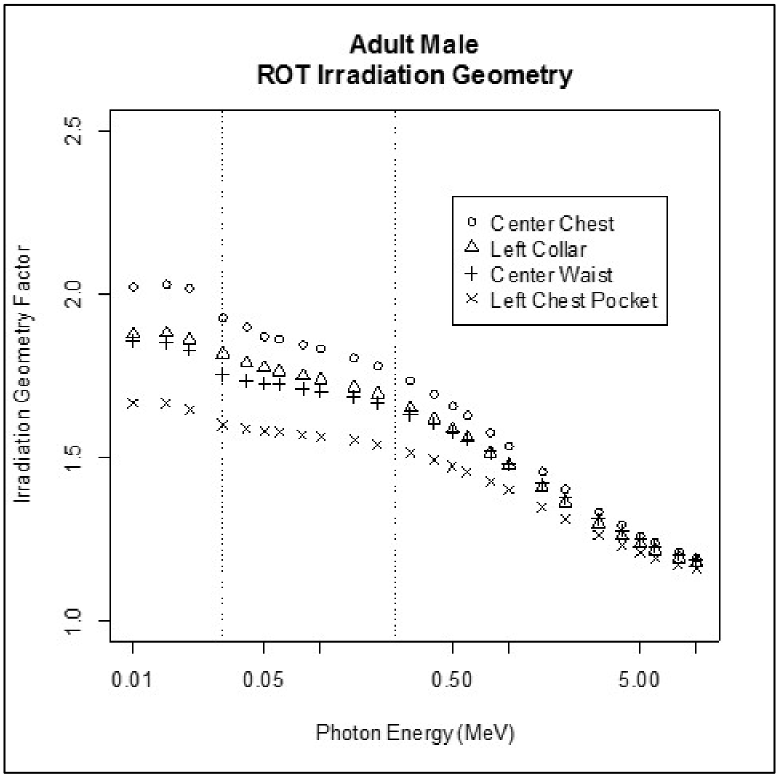

Figure 3-3. IGFs for uncollided photons in dosimeter regions when the adult male voxel phantom is irradiated in the ROT geometry by monoenergetic photons.

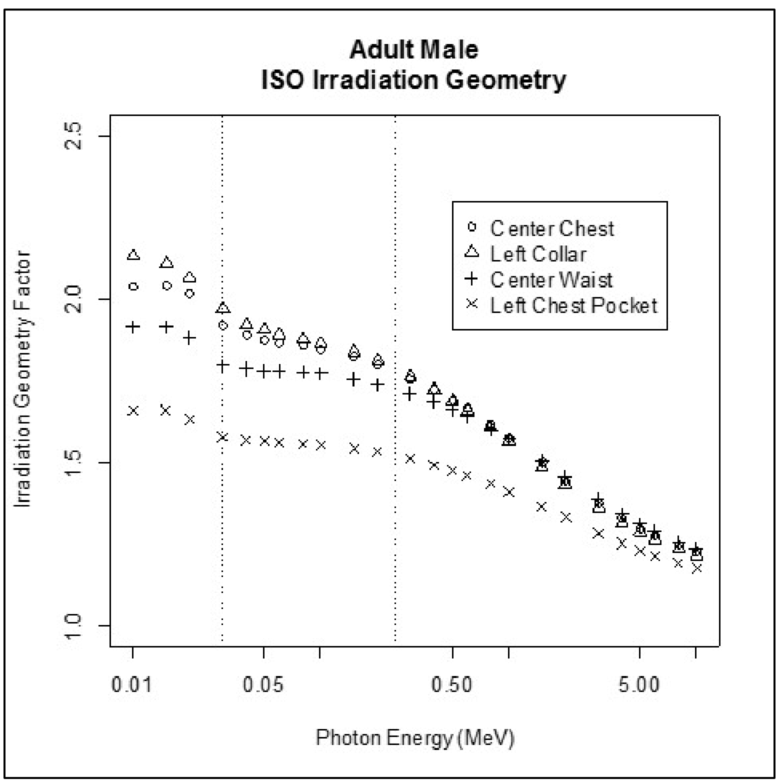

Figure 3-4. IGFs for uncollided photons in dosimeter regions when the adult male voxel phantom is irradiated in the ISO geometry by monoenergetic photons.

Table 3-1. Estimated ROT IGFs for monoenergetic photons incident on a voxel phantom.

Dosimeter position	Energy regions and estimated IGFs for *Hp(10)*, adult female phantom		Energy regions and estimated IGFs for *Hp(10)*, adult male phantom	
Center chest	≤30 keV:	2.02	≤30 keV:	2.00
	30–250 keV:	1.77	30–250 keV:	1.84
	>250 keV:	1.37	>250 keV:	1.44
Left collar	≤30 keV:	1.97	≤30 keV:	1.86
	30–250 keV:	1.79	30–250 keV:	1.75
	>250 keV:	1.40	>250 keV:	1.40
Center waist	≤30 keV:	1.78	≤30 keV:	1.82
	30–250 keV:	1.65	30–250 keV:	1.71
	>250 keV:	1.35	>250 keV:	1.40
Left chest pocket	≤30 keV:	1.56	≤30 keV:	1.65
	30–250 keV:	1.49	30–250 keV:	1.57
	>250 keV:	1.27	>250 keV:	1.33
Average of four dosimeter locations	≤30 keV:	1.83	≤30 keV:	1.83
	30–250 keV:	1.68	30–250 keV:	1.72
	>250 keV:	1.35	>250 keV:	1.39

Table 3-2. Estimated ISO IGFs for monoenergetic photons incident on a voxel phantom.

Dosimeter position	Energy regions and estimated IGFs for *Hp(10)*, adult female phantom		Energy regions and estimated IGFs for *Hp(10)*, adult male phantom	
Center chest	≤30 keV:	1.96	≤30 keV:	2.00
	30–250 keV:	1.76	30–250 keV:	1.85
	>250 keV:	1.42	>250 keV:	1.54
Left collar	≤30 keV:	2.18	≤30 keV:	2.07
	30–250 keV:	1.91	30–250 keV:	1.87
	>250 keV:	1.46	>250 keV:	1.53
Center waist	≤30 keV:	1.82	≤30 keV:	1.88
	30–250 keV:	1.71	30–250 keV:	1.77
	>250 keV:	1.43	>250 keV:	1.53
Left chest pocket	≤30 keV:	1.57	≤30 keV:	1.63
	30–250 keV:	1.48	30–250 keV:	1.55
	>250 keV:	1.28	>250 keV:	1.40
Average of four dosimeter locations	≤30 keV:	1.88	≤30 keV:	1.90
	30–250 keV:	1.71	30–250 keV:	1.76
	>250 keV:	1.40	>250 keV:	1.50

3.2.2 NEUTRON IRRADIATIONS

Pointwise estimates of the IGFs for neutrons are shown in Figures 3-5 through 3-8. In the figures, the dotted vertical lines show the boundaries of the IREP dose groupings.

The IGF factors for neutrons that irradiated the voxel phantoms in the ROT irradiation geometry, averaged over the IREP energy regions, are listed in Table 3-3. The IGF factors for photons that irradiated the voxel phantoms in the ISO irradiation geometry, averaged over the IREP energy regions, are listed in Table 3-4.

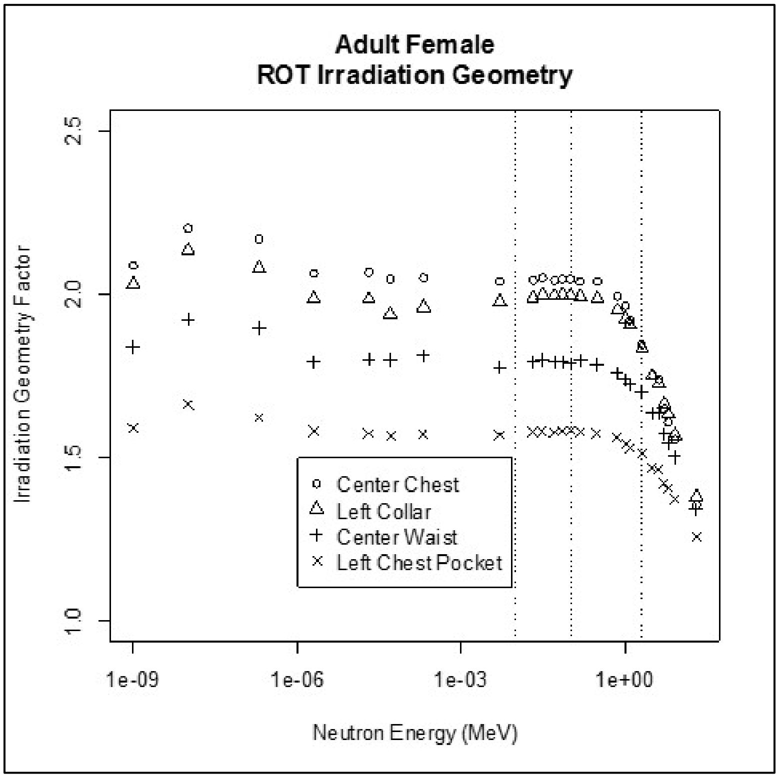

Figure 3-5. IGFs for uncollided neutrons in dosimeter regions when the adult female voxel phantom is irradiated in the ROT geometry by monoenergetic neutrons.

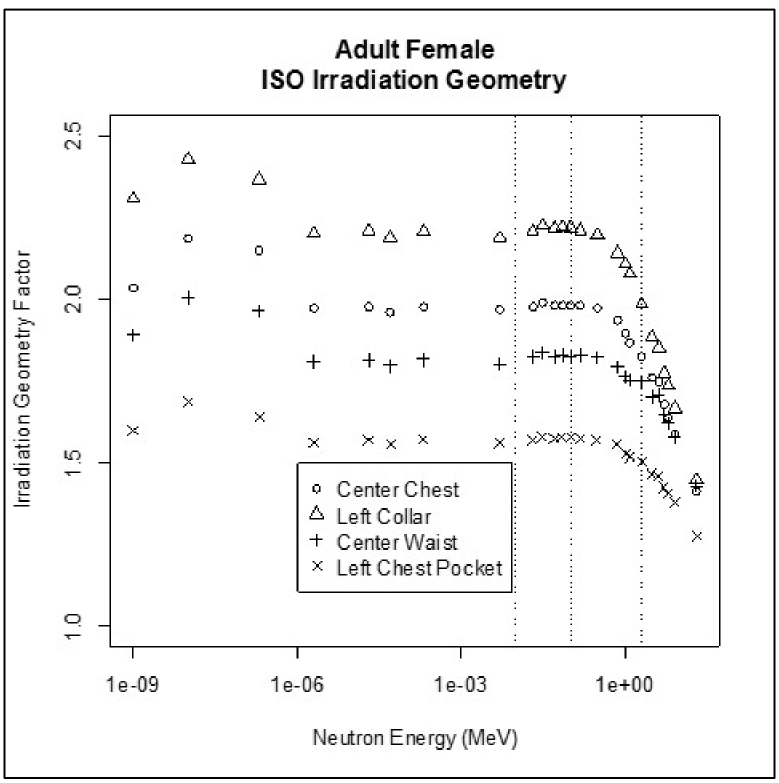

Figure 3-6. IGFs for uncollided neutrons in dosimeter regions when the adult female voxel phantom is irradiated in the ISO geometry by monoenergetic neutrons.

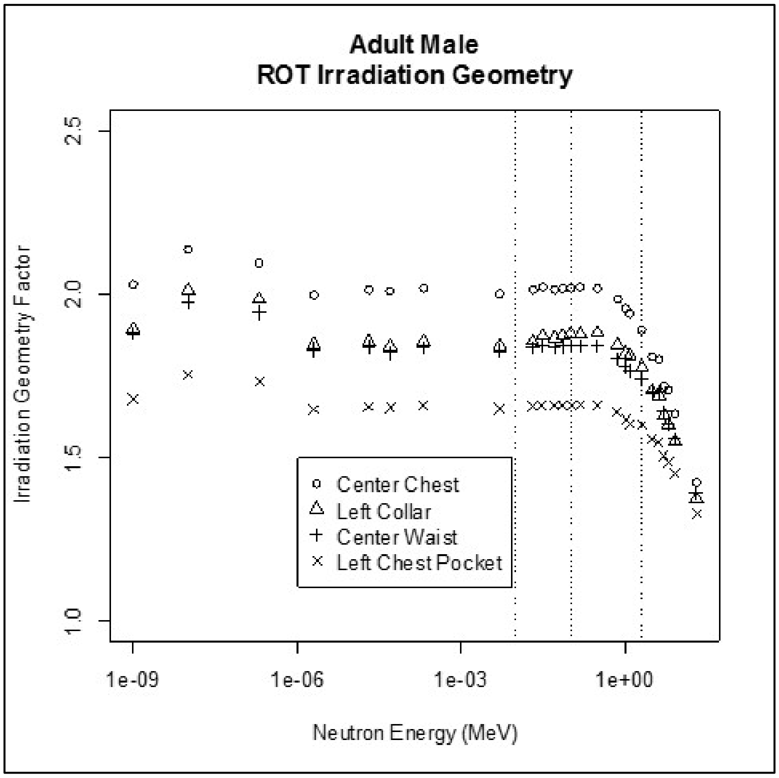

Figure 3-7. IGFs for uncollided neutrons in dosimeter regions when the adult male voxel phantom is irradiated in the ROT geometry by monoenergetic neutrons.

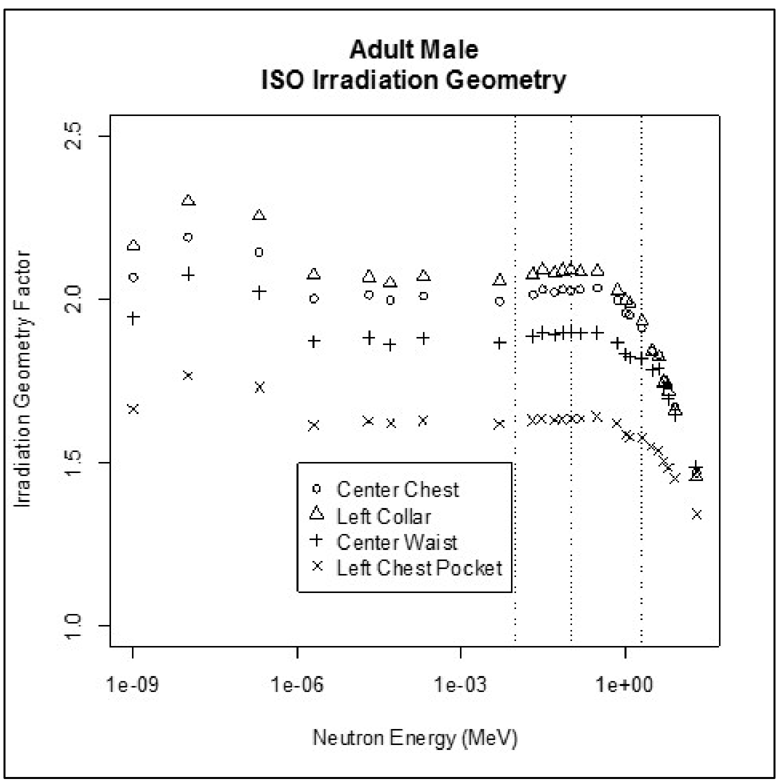

Figure 3-8. IGFs for uncollided neutrons in dosimeter regions when the adult male voxel phantom is irradiated in the ISO geometry by monoenergetic neutrons.

Table 3-3. Estimated ROT IGFs for monoenergetic neutrons incident on a voxel phantom.

Dosimeter position	Energy regions and estimated IGFs for *Hp(10)*, adult female phantom		Energy regions and estimated IGFs for *Hp(10)*, adult male phantom	
Center chest	≤10 keV:	1.68	≤10 keV:	1.74
	10–100 keV:	2.02	10–100 keV:	2.00
	100 keV–2 MeV:	2.04	100 keV–2 MeV:	2.02
	2–20 MeV:	2.11	2–20 MeV:	2.05
Left collar	≤10 keV:	1.68	≤10 keV:	1.64
	10–100 keV:	1.97	10–100 keV:	1.86
	100 keV–2 MeV:	1.99	100 keV–2 MeV:	1.86
	2–20 MeV:	2.03	2–20 MeV:	1.90
Center waist	≤10 keV:	1.58	≤10 keV:	1.64
	10–100 keV:	1.77	10–100 keV:	1.82
	100 keV–2 MeV:	1.79	100 keV–2 MeV:	1.84
	2–20 MeV:	1.84	2–20 MeV:	1.88
Left chest pocket	≤10 keV:	1.43	≤10 keV:	1.51
	10–100 keV:	1.57	10–100 keV:	1.65
	100 keV–2 MeV:	1.58	100 keV–2 MeV:	1.66
	2–20 MeV:	1.60	2–20 MeV:	1.69
Average of four dosimeter locations	≤10 keV:	1.59	≤10 keV:	1.63
	10–100 keV:	1.83	10–100 keV:	1.83
	100 keV–2 MeV:	1.85	100 keV–2 MeV:	1.84
	2–20 MeV:	1.89	2–20 MeV:	1.88

Table 3-4. Estimated ISO IGFs for monoenergetic neutrons incident on a voxel phantom.

Dosimeter position	Energy regions and estimated IGFs for *Hp(10)*, adult female phantom		Energy regions and estimated IGFs for *Hp(10)*, adult male phantom	
Center chest	≤10 keV:	1.69	≤10 keV:	1.77
	10–100 keV:	1.95	10–100 keV:	2.01
	100 keV–2 MeV:	1.98	100 keV–2 MeV:	2.02
	2–20 MeV:	2.05	2–20 MeV:	2.07
Left collar	≤10 keV:	1.80	≤10 keV:	1.77
	10–100 keV:	2.17	10–100 keV:	2.06
	100 keV–2 MeV:	2.21	100 keV–2 MeV:	2.08
	2–20 MeV:	2.28	2–20 MeV:	2.15
Center waist	≤10 keV:	1.65	≤10 keV:	1.72
	10–100 keV:	1.81	10–100 keV:	1.88
	100 keV–2 MeV:	1.82	100 keV–2 MeV:	1.89
	2–20 MeV:	1.88	2–20 MeV:	1.94
Left chest pocket	≤10 keV:	1.43	≤10 keV:	1.50
	10–100 keV:	1.56	10–100 keV:	1.62
	100 keV–2 MeV:	1.57	100 keV–2 MeV:	1.63
	2–20 MeV:	1.60	2–20 MeV:	1.67
Average of four dosimeter locations	≤10 keV:	1.64	≤10 keV:	1.69
	10–100 keV:	1.87	10–100 keV:	1.89
	100 keV–2 MeV:	1.90	100 keV–2 MeV:	1.90
	2–20 MeV:	1.95	2–20 MeV:	1.96

3.3 ANGULAR RESPONSE

The data above show that the IGFs for the left chest pocket are always low. The reason for this is the location of the dosimeter to the left side of the phantom. Figure 3-9 shows the particle fluence (in arbitrary units) from 200-keV photons at the four dosimeter locations as the radiation source rotates around the adult male phantom. The angles are measured from the Cartesian *y*-axis so the source at 0 degrees gives an AP irradiation geometry. The angular response of the three dosimeters located on, or near, the centerline of the phantom, center chest, center waist, and left collar are shown. As would be expected, there is a steep decline in the calculated photon fluence when the incident photons are started from a region behind the phantom (angles between π/2 and 3π/2 radians). The left chest pocket dosimeter is offset to the left (see Figures A-8 and B-2), which results in it being irradiated to a greater extent than for the other three dosimeter locations at angles between 90 and 135 degrees (π/2 and 3π/4 radians) as can be seen in Figure 3-9. The enhanced irradiation of the left chest pocket dosimeter is the reason that the IGFs of the left chest dosimeter location are lower than those for the other three dosimeter locations.

The data in Figure 3-9 show that the assumption of an AP irradiation geometry provides the correct fluence even if the rotational angle deviates from the AP irradiation geometry by up to ±75 degrees (±5/6π radians). The data also show that, except for the left chest pocket dosimeter location at the incident angles mentioned above, the particle fluence at the dosimeter location does not vary greatly with dosimeter location.

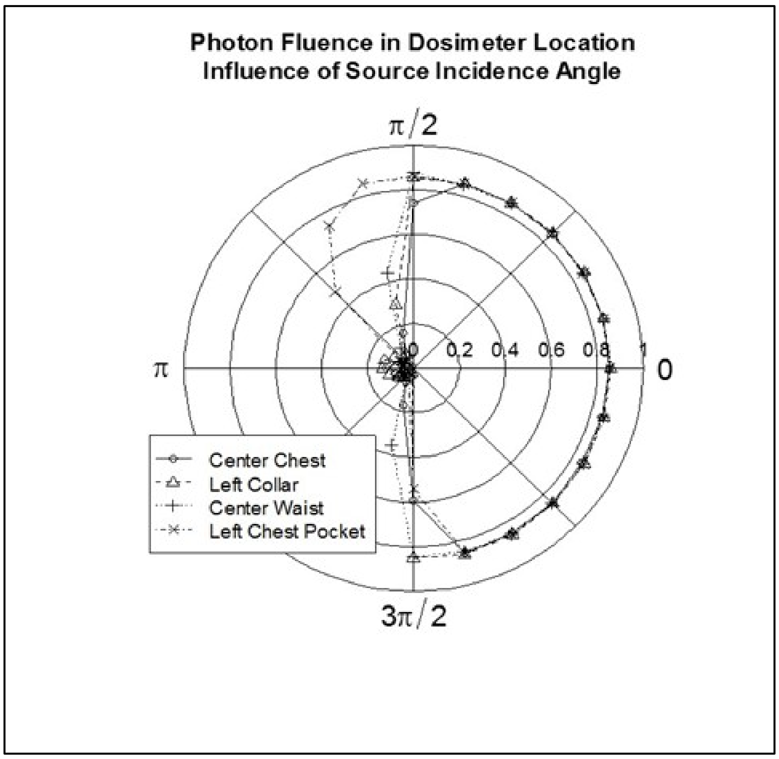

Figure 3-9. Rotational dependence of fluence at four dosimeter locations for uncollided 0.2-MeV photons.

4.0 DISCUSSION

These preliminary factors indicate that, within the selected energy bins, the male and female IGFs are nearly equal. The factors also show that they vary according to the location of the dosimeter but that the dependence is not large, except for the left chest pocket location, and that an IGF based on the center chest location will tend to be favorable to claimants.

The factors described above do not account for the angular response of the dosimeter that might be worn by the worker but only represents the radiation that is available to the dosimeter. The factors also do not account for the efficiencies of any particular dosimeter and, in particular, do not account for the response of the dosimeter to albedo radiation. The albedo and angular response of site dosimeters should be considered when documenting the appropriate IGFs in the technical basis documents and dose reconstruction tools and methods, which should provide appropriate direction.

5.0 SUMMARY

IGFs that account for the reduction in apparent particle fluence to which dosimeters are exposed in the ROT and ISO geometries were calculated. The factors vary according to dosimeter location on the body and the energy of the particles that irradiate the body. The factors for male and female phantoms are similar. The factors tend to decrease as the particle energy increases. A dosimeter placed on the center chest tends to result in the largest (most favorable to claimants) DCC.

REFERENCES

González, Á., 2009, "Measurement of Areas on a Sphere Using Fibonacci and Latitude–Longitude Lattices," *Mathematical Geosciences*, volume 42, pp. 49–64. [SRDB Ref ID: 154005]

Hannay, J. H., and J. F. Nye, 2004, "Fibonacci Numerical Integration on a Sphere," *Journal of Physics A: Mathematical and General*, volume 37, number 48, pp. 11591–11601. [SRDB Ref ID: 154003]

ICRP (International Commission on Radiological Protection), 1987, *Data for Use in Protection Against External Radiation*, Publication 51, Pergamon Press, Oxford, England. [SRDB Ref ID: 135826]

ICRP (International Commission on Radiological Protection), 1996, *Conversion Coefficients for Use in Radiological Protection Against External Radiation*, Publication 74, Pergamon Press, Oxford, England. [SRDB Ref ID: 7979]

ICRP (International Commission on Radiological Protection), 2009, *Adult Reference Computational Phantoms*, Publication 110, Pergamon Press, Oxford, England.

ICRP (International Commission on Radiological Protection), 2010, *Conversion Coefficients for Radiological Protection Quantities for External Radiation Exposures*, Publication 116, Elsevier Press, Philadelphia, Pennsylvania.

LANL (Los Alamos National Laboratory), 2011, "Interpreted ENDF File for ENDFB-VII.1-neutron/O/16" downloaded from the T-2 Nuclear Information Service http://t2.lanl.gov/nis/data/data/ENDFB-VII.1-neutron/O/16 on 8-Feb-2016. Los Alamos National Security, Los Alamos, New Mexico. [SRDB Ref ID: 154073]

NIOSH (National Institute for Occupational Safety and Health), 2007, *External Dose Reconstruction Implementation Guideline*, OCAS-IG-001, Rev. 3, Office of Compensation Analysis and Support, Cincinnati, Ohio, November 21.

Pelowitz, D. B., editor, 2013, *MCNP6^{TM} User's Manual*, Version 1.0, LA-CP-13-00634, Rev. 0., Los Alamos National Laboratory, Los Alamos, New Mexico.

RDCT (R Development Core Team), 2014, *R: A Language and Environment for Statistical Computing, Reference Index*, R Foundation for Statistical Computing, Vienna, Austria, April 14.

SC&A (Sanford Cohen & Associates), 2005, *The Review of NIOSH/ORAUT Procedures and Methods Used for Dose Reconstruction*, SCA-TR-Task3, Rev. 0, McLean, Virginia, January 17. [SRDB Ref ID: 137643]

Swinbank, R., and R. J. Purser, 2006, "Fibonacci Grids: A Novel Approach to Global Modeling," *Quarterly Journal of the Royal Meteorological Society*, volume 132, number 619, pp. 1769–1793. [SRDB Ref ID: 154072]

Thierry-Chef, I., F. Pernicka, M. Marshall, E. Cardis, and P. Andreo, 2002, "Study of a Selection of 10 Historical Types of Dosemeter: Variation of the Response to $H_p(10)$ with Photon Energy and Geometry of Exposure," *Radiation Protection Dosimetry*, volume 102, number 2, pp. 101–113. [SRDB Ref ID: 11296]

ATTACHMENT A
DOSIMETER LOCATIONS ON THE ADULT FEMALE VOXEL PHANTOM

LIST OF FIGURES

FIGURES	TITLE	PAGE
A-1	Elevation view of the adult female voxel phantom showing the center chest dosimeter location	21
A-2	Plan view of the adult female voxel phantom showing the center chest dosimeter location	22
A-3	Elevation view of the adult female voxel phantom showing the left collar dosimeter location	22
A-4	Plan view of the adult female voxel phantom showing the left collar dosimeter location	23
A-5	Elevation view of the adult female voxel phantom showing the center waist dosimeter location	23
A-6	Plan view of the adult female voxel phantom showing the center waist dosimeter location	24
A-7	Elevation view of the adult female voxel phantom showing the left chest pocket dosimeter location	25
A-8	Plan view of the adult female voxel phantom showing the left chest pocket dosimeter location	26

ATTACHMENT A
DOSIMETER LOCATIONS ON THE ADULT FEMALE VOXEL PHANTOM (continued)

The locations of the dosimeters on the adult female voxel phantom are shown in this attachment. The dosimeters are the clear areas shown on the phantom, which consists of many voxels. The grid lines in the figures are the surface lines of the individual voxels. Shaded voxels are those that contain tissue materials; unshaded voxels do not contain any material. The dosimeters shown in the figures are also empty as described in Section 2.2 of the report.

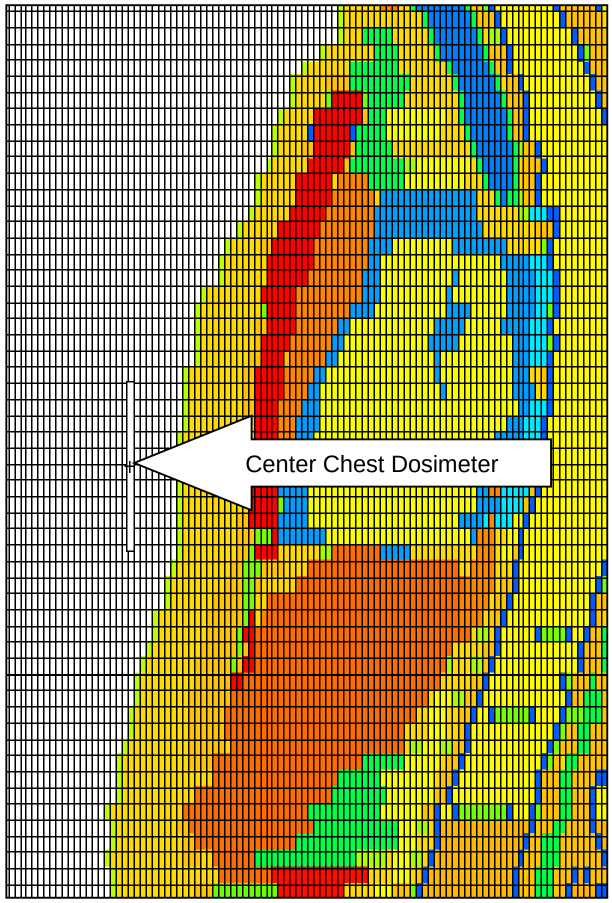

Figure A-1. Elevation view of the adult female voxel phantom showing the center chest dosimeter location.

ATTACHMENT A
DOSIMETER LOCATIONS ON THE ADULT FEMALE VOXEL PHANTOM (continued)

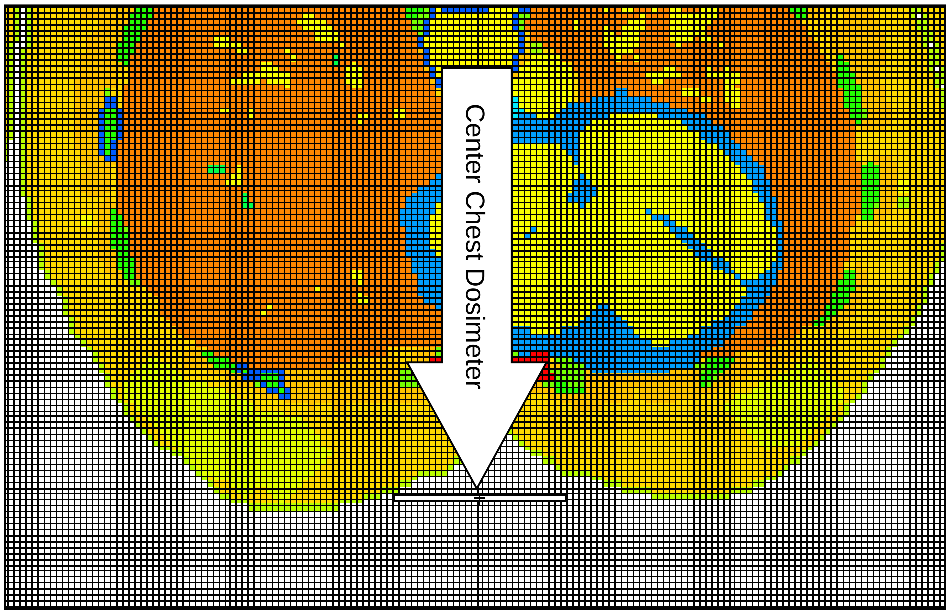

Figure A-2. Plan view of the adult female voxel phantom showing the center chest dosimeter location.

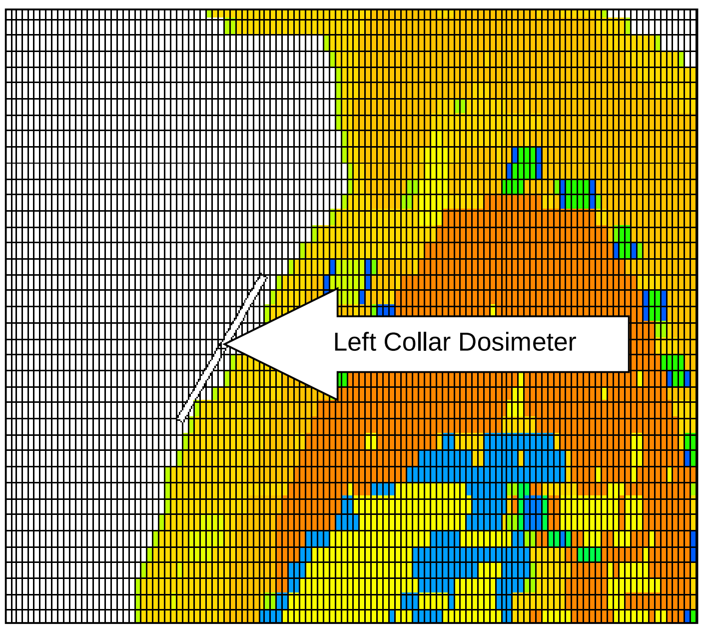

Figure A-3. Elevation view of the adult female voxel phantom showing the left collar dosimeter location.

ATTACHMENT A
DOSIMETER LOCATIONS ON THE ADULT FEMALE VOXEL PHANTOM (continued)

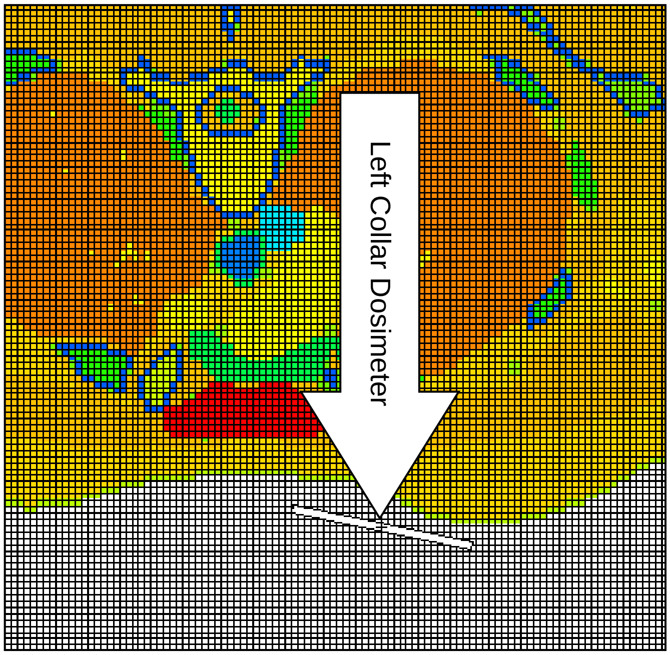

Figure A-4. Plan view of the adult female voxel phantom showing the left collar dosimeter location.

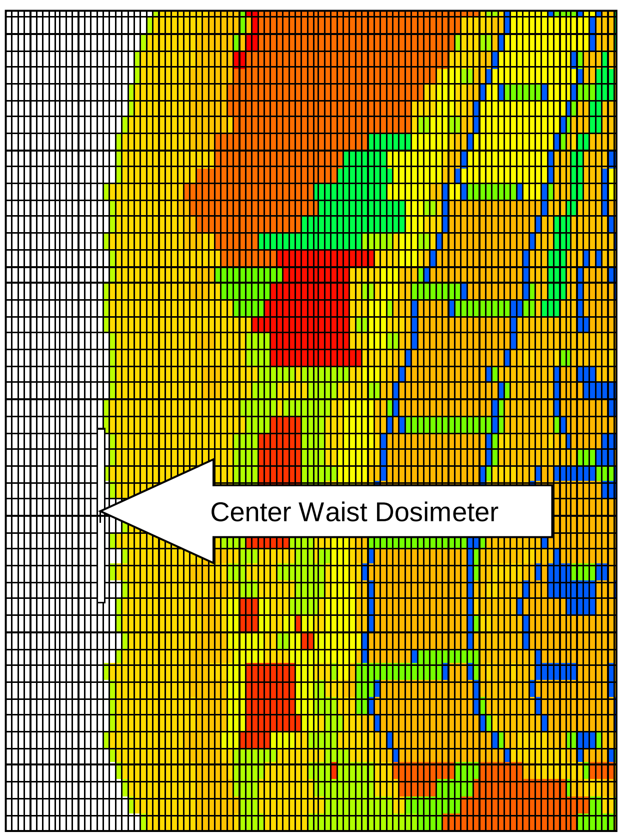

Figure A-5. Elevation view of the adult female voxel phantom showing the center waist dosimeter location.

ATTACHMENT A
DOSIMETER LOCATIONS ON THE ADULT FEMALE VOXEL PHANTOM (continued)

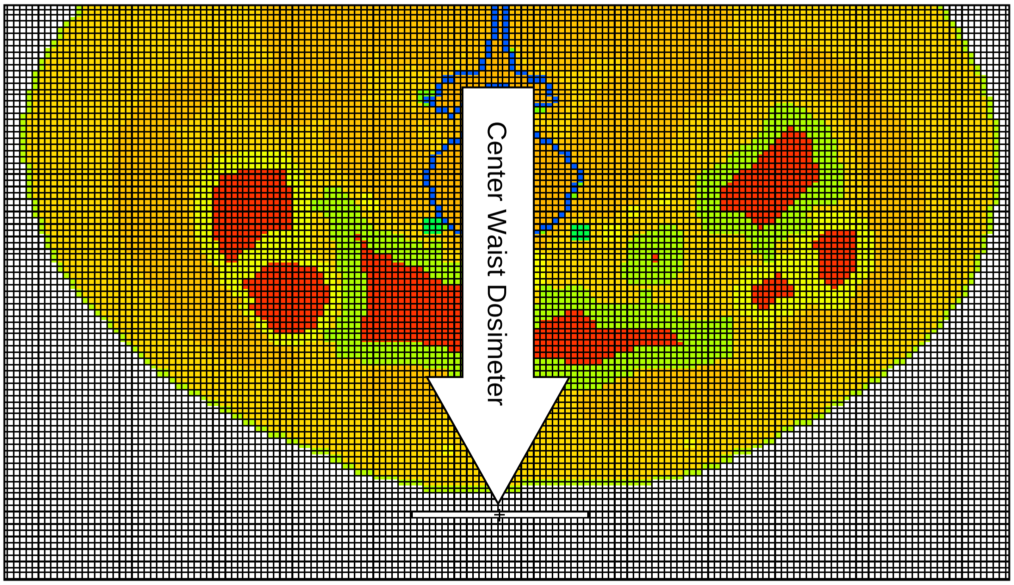

Figure A-6. Plan view of the adult female voxel phantom showing the center waist dosimeter location.

ATTACHMENT A
DOSIMETER LOCATIONS ON THE ADULT FEMALE VOXEL PHANTOM (continued)

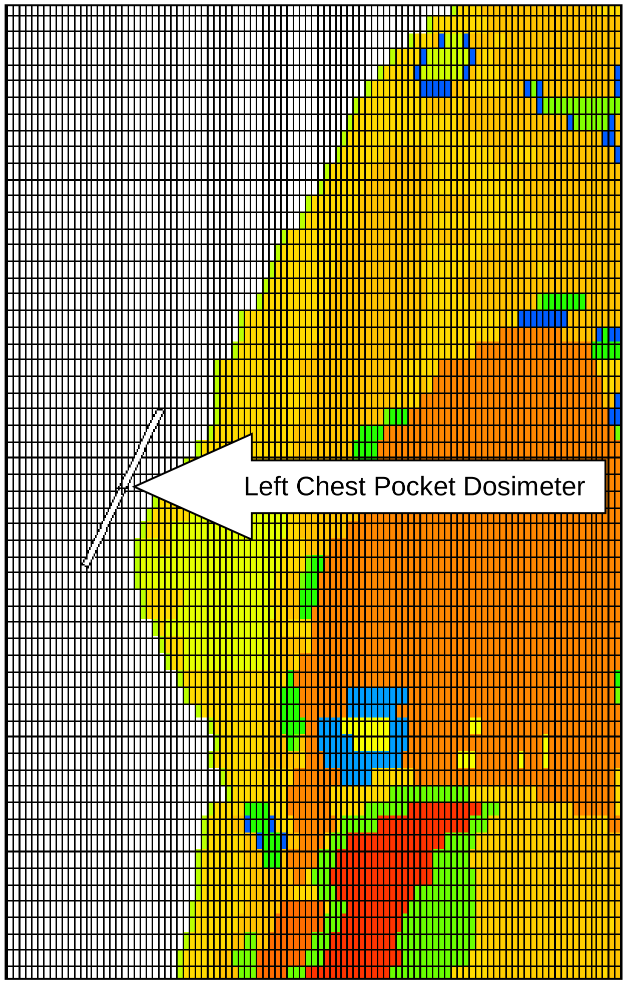

Figure A-7. Elevation view of the adult female voxel phantom showing the left chest pocket dosimeter location.

ATTACHMENT A
DOSIMETER LOCATIONS ON THE ADULT FEMALE VOXEL PHANTOM (continued)

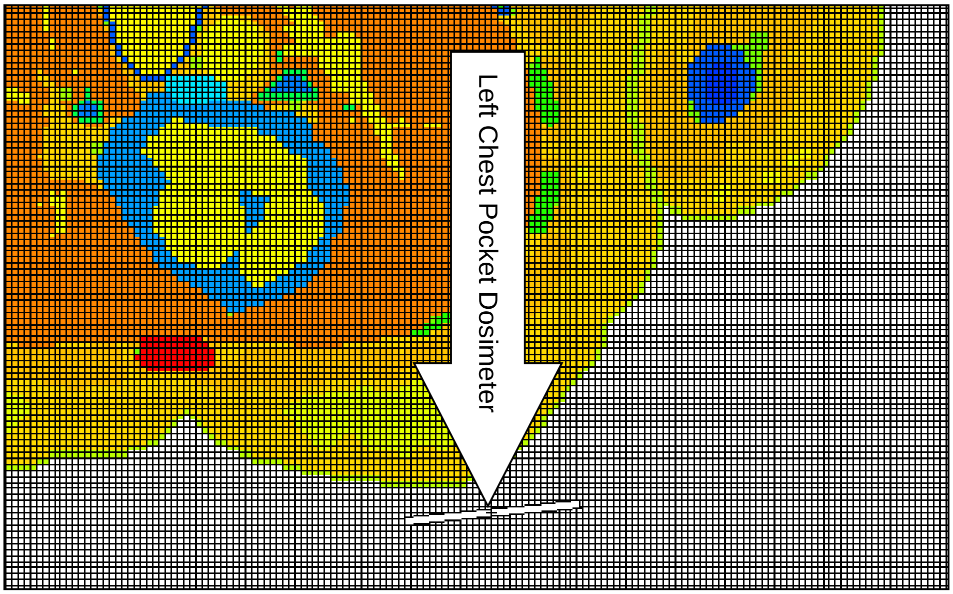

Figure A-8. Plan view of the adult female voxel phantom showing the left chest pocket dosimeter location.

ATTACHMENT B
DOSIMETER LOCATIONS ON THE ADULT MALE VOXEL PHANTOM

LIST OF FIGURES

FIGURES	TITLE	PAGE
B-1	Elevation view of the adult male voxel phantom showing the center chest and center waist dosimeter locations	28
B-2	Plan view of the adult male voxel phantom showing the center chest and left chest pocket dosimeter locations	29
B-3	Plan view of the adult male voxel phantom showing the center waist dosimeter location	29
B-4	Plan view of adult male voxel phantom showing the left collar dosimeter	30
B-5	Elevation view of the adult male voxel phantom showing the left collar dosimeter location	30
B-6	Elevation view of the adult male voxel phantom showing the left chest pocket dosimeter location	31

ATTACHMENT B
DOSIMETER LOCATIONS ON THE ADULT MALE VOXEL PHANTOM (continued)

The locations of the dosimeters on the adult male voxel phantom are shown in this attachment. The dosimeters are the clear areas shown on the phantom, which consists of many voxels. The grid lines in the figures are the surface lines of the individual voxels. Shaded voxels are those that contain tissue materials; unshaded voxels do not contain any material. The dosimeters shown in the figures are also empty as described in Section 2.2 of the report.

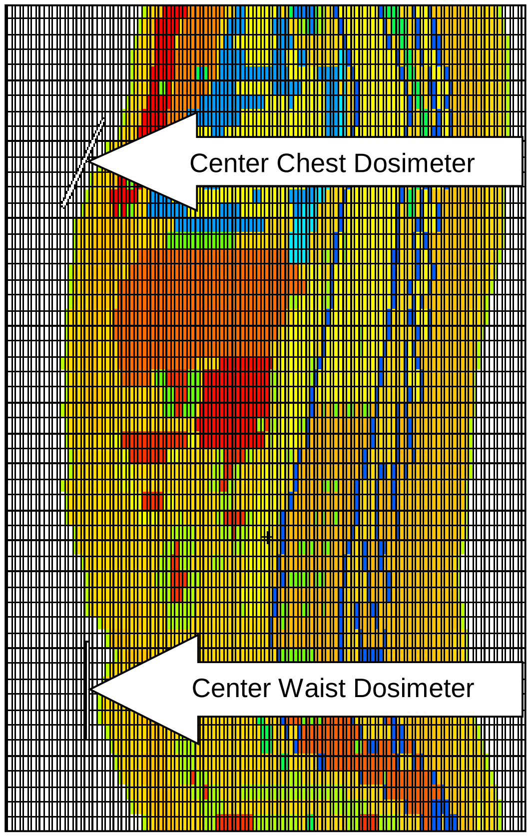

Figure B-1. Elevation view of the adult male voxel phantom showing the center chest and center waist dosimeter locations.

ATTACHMENT B
DOSIMETER LOCATIONS ON THE ADULT MALE VOXEL PHANTOM (continued)

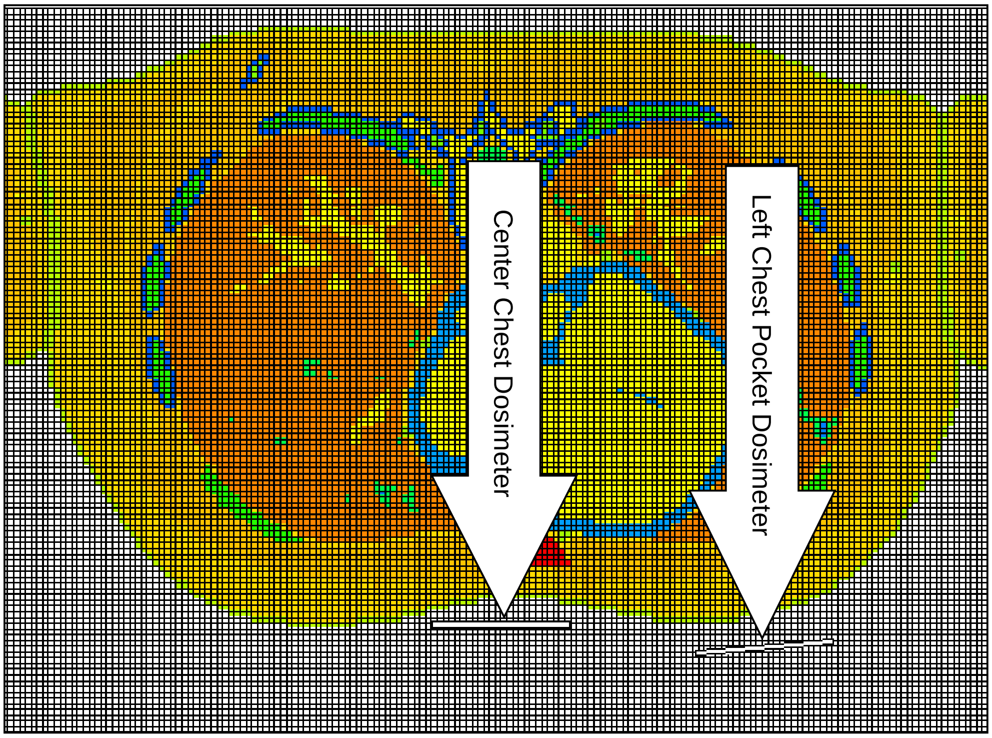

Figure B-2. Plan view of the adult male voxel phantom showing the center chest and left chest pocket dosimeter locations.

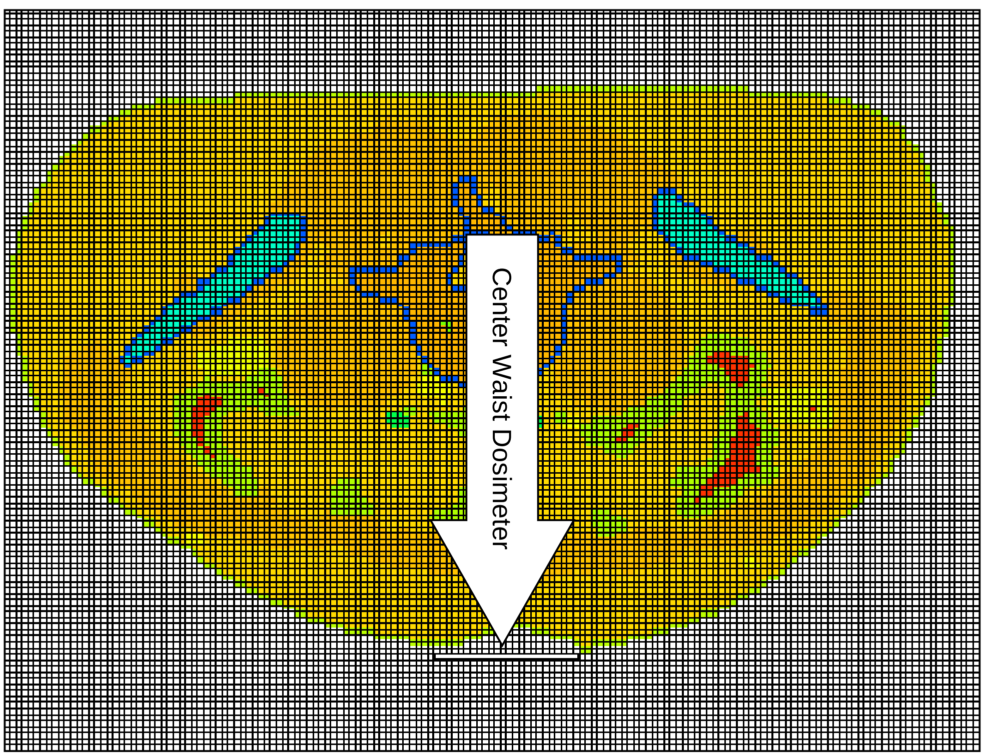

Figure B-3. Plan view of the adult male voxel phantom showing the center waist dosimeter location.

ATTACHMENT B
DOSIMETER LOCATIONS ON THE ADULT MALE VOXEL PHANTOM (continued)

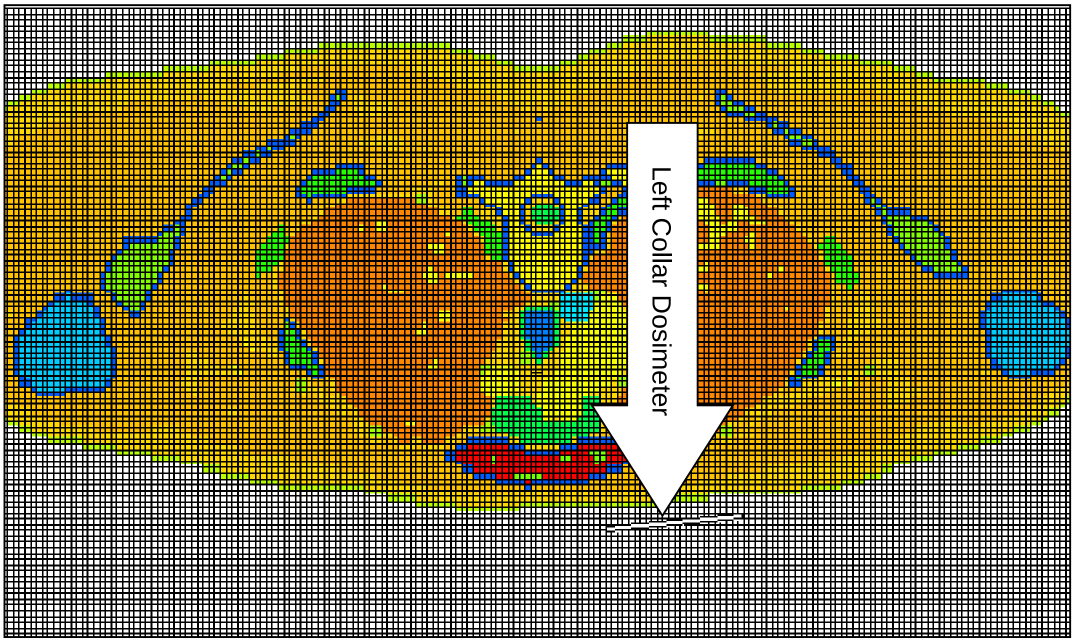

Figure B-4. Plan view of adult male voxel phantom showing the left collar dosimeter.

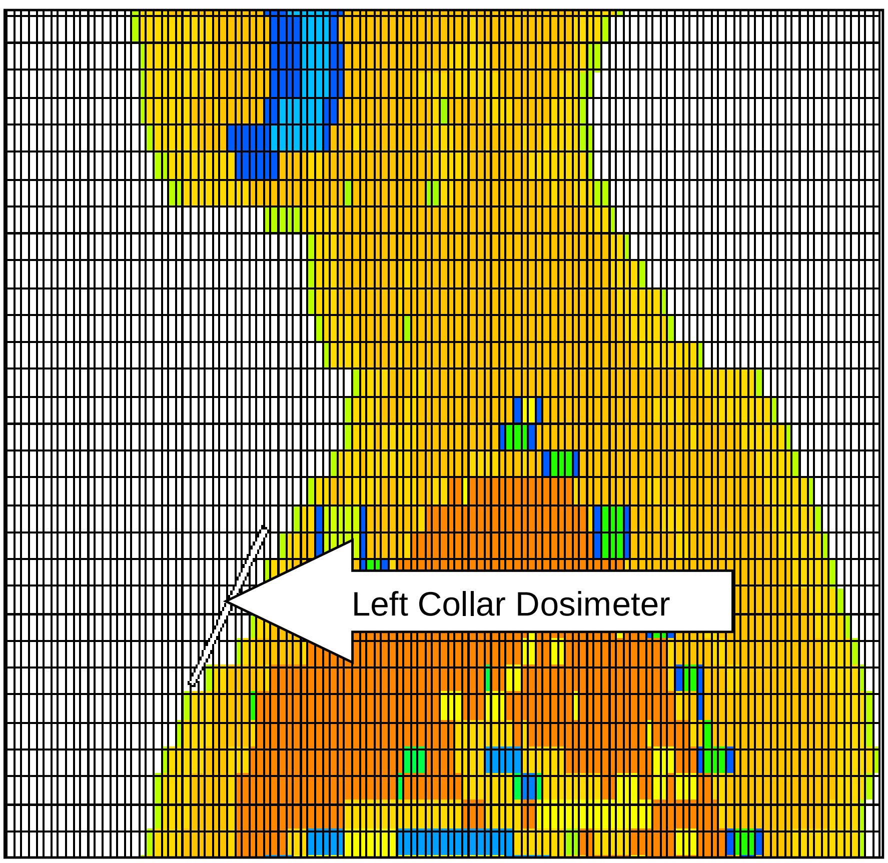

Figure B-5. Elevation view of the adult male voxel phantom showing the left collar dosimeter location.

ATTACHMENT B
DOSIMETER LOCATIONS ON THE ADULT MALE VOXEL PHANTOM (continued)

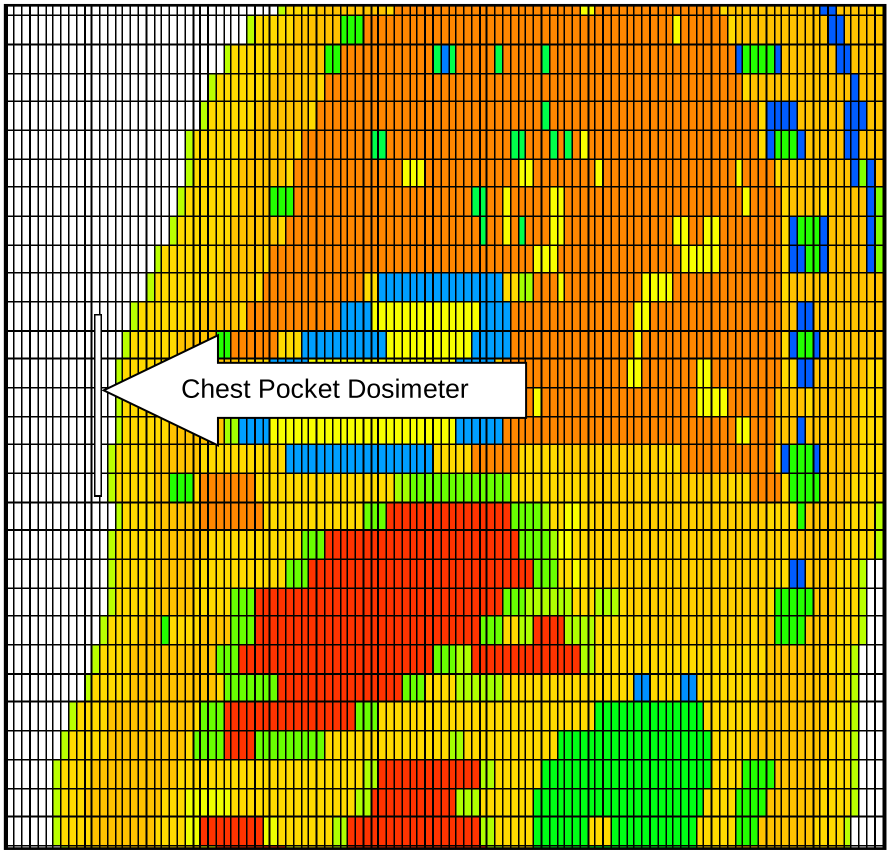

Figure B-6. Elevation view of the adult male voxel phantom showing the left chest pocket dosimeter location.

ATTACHMENT C
EXAMPLE MCNP6 INPUT FILE

This attachment contains one example of the MCNP6.1 input files that were used for this report. The example input file is for an adult male phantom irradiated by an aligned and expanded beam of 0.3-MeV neutrons at discrete angles that range from 0 to 355 degrees in 5-degree increments. The input file implements the ROT irradiation geometry. The “fill” card has been edited to remove 29,277 lines of the original file.

```
RPT068.AM_Ns_M110_E00300_ROT_.80c.i
  c
  c
  c  ***************************************************************************
  c  |                      File Description Section                           |
  c  ---------------------------------------------------------------------------
  c
  c       Date:        18-Mar-2015
  c
  c       Author:      Richard J. Traub, PhD
  c                    Dade Moeller & Assoc
  c                    1835 Terminal Drive #200
  c                    Richland WA 99354
  c                    509.942.3732
  c
  c       Client:      NIOSH/ORAU
  c
  c       File Name Information
  c
  c    RPT068.AM_N__M110_E00300_ROT_.80c.i
  c
  c    RPT068        : This file calculates the particle fluence in dosimeters
  c                    located on the center of the chest, hanging from the left
  c                    collar of a shirt, at the center of the waist (belt buckle),
  c                    and at the left chest pocket of a lab coat.
  c                    The geometry is a voxel phantom (nose pointing in
  c                    Y-negative direction).  The phantom is irradiated
  c                    by a monoenergetic neutron source (aligned and expanded)
  c                    That is rotated around the Z-axis by the angle specified
  c                    by the R___ definition.
  c       AM         : ICRP V1.1 Adult Male Phantom
  c       Ns         : Neutron Source + S(alpha,beta) treatment
  c       M110       : mode n p (n p e)
  c       E00300     :  ( 0.3 MeV)
  c       ROT_       : Door Source Rotation:
  c                       72 rotations in 5 deg increments around Z-Axis
  c       80c        : MCNP6.1 default (ENDF/B-VII.1)
  c
  c
  c
  c  ***************************************************************************
  c  |                      Cell Definition Section                            |
  c  ---------------------------------------------------------------------------
  c
  c
200  0    -200    imp:n,p=1  trcl=200  $  dosimeter on center chest
201  like 200 but trcl=201           $  dosimeter on left collar
202  like 200 but trcl=202           $  dosimeter on center waist
203  like 200 but trcl=203           $  dosimeter on left chest pocket
  c
c   300  0    -300      imp:n,p=1         $  Source Box
  c
  c  Begin Lattice [% Voxel Phantom %]
  c    Bounding Container: U=0, filled by U=996
8    0   -1    #200 #201 #202 #203                     fill=996 imp:n,p=1  $
  c
  c    Lattice Unit Cell:  U=996, Filled by U=(1..141,256)
7    0   -2    lat = 1 u = 996 imp:n,p=1               $ individual lattice cells
                 fill = 0:253  0:126 0:221
  c
  c
```

ATTACHMENT C
EXAMPLE MCNP6 INPUT FILE (continued)

```
c  ============================================================================
c  BEGIN:  Fill Cards for ICRP-110 Adult Male Voxel Phantom
c  ============================================================================
c
c  File: ICRP110_AM_MCNPfill.txt
c
c  This file contains the ICRP-110 Adult Male Voxel Phantom
c
c  The zero "0" entries of the ICRP AM.dat file have been converted to
c   "256" to avoid problems that occur when Fill=0.
c  The data entries have been converted to a compact format that facilitates
c    reading of the file by Vised 24E.  The "tissue type" data entries of the
c    original AM.dat file have been retained.
c
c  In the ICRP distribution
c   void voxels are designated with zero "0".  In this file,
c   void voxels are designated with 256.  The universe numbers in
c   this file are [1..141,256].
c
c  The dimensions of the AM voxel are:
c    0.2137 cm * 0.2137 cm * 0.800 cm = 0.036534 cm^3
c
c        nRows = 127
c        nCols = 254
c        nSli  = 222
c        nVox  = 7 161 276
c
   256 1856r 141 5r 256 246r 141 7r 256 245r 141 8r 256 244r 141 9r 256
   243r 141 9r 256 243r 141 10r 256 242r 141 10r 256 243r 141 9r 256
   *
   *  29,277 lines deleted
   *  consider the entry pair "256 243r"
   *  material "256" fills the lattice cell
   *  "243r" means the next 243 lattice cells are also filled with
   *  material "256"
   *
   27r 256 226r 141 25r 256 227r 141 25r 256 228r 141 23r 256 229r 141
   23r 256 229r 141 23r 256 230r 141 21r 256 233r 141 17r 256 236r 141
   14r 256 239r 141 10r 256 10029r
c
c  ============================================================================
c  END:  Fill Cards for ICRP-110 Adult Male Voxel Phantom
c  ============================================================================
c
c
c  ============================================================================
c  BEGIN:  Cell/Universe Cards for ICRP-110 Adult Male Voxel Phantom
c  ============================================================================
c
c  File:  ICRP110_AM.Material_Universes.R01.txt
c
c  Universes for the ICRP-110 Adult Male Voxel Phantoms
c   Includes U=256 as a void (the zero "0" tissue of AM.dat)
c   Note:  imp:e=1 has been commented out
c
22    43  -1.030 -3   u=1    imp:n,p=1 $ imp:e=1  $  Adrenal, left
23    43  -1.030 -3   u=2    imp:n,p=1 $ imp:e=1  $  Adrenal, right
24    45  -1.030 -3   u=3    imp:n,p=1 $ imp:e=1  $  Anterior nasal passage (ET1)
25    45  -1.030 -3   u=4    imp:n,p=1 $ imp:e=1  $  Posterior nasal passage down to larynx (ET2)
26    29  -1.050 -3   u=5    imp:n,p=1 $ imp:e=1  $  Oral mucosa, tongue
27    29  -1.050 -3   u=6    imp:n,p=1 $ imp:e=1  $  Oral mucosa, lips and cheeks
28    45  -1.030 -3   u=7    imp:n,p=1 $ imp:e=1  $  Trachea
29    45  -1.030 -3   u=8    imp:n,p=1 $ imp:e=1  $  Bronchi
30    28  -1.060 -3   u=9    imp:n,p=1 $ imp:e=1  $  Blood vessels, head
31    28  -1.060 -3   u=10   imp:n,p=1 $ imp:e=1  $  Blood vessels, trunk
32    28  -1.060 -3   u=11   imp:n,p=1 $ imp:e=1  $  Blood vessels, arms
33    28  -1.060 -3   u=12   imp:n,p=1 $ imp:e=1  $  Blood vessels, legs
34     2  -1.920 -3   u=13   imp:n,p=1 $ imp:e=1  $  Humeri, upper half, cortical
35     3  -1.205 -3   u=14   imp:n,p=1 $ imp:e=1  $  Humeri, upper half, spongiosa
36    22  -0.980 -3   u=15   imp:n,p=1 $ imp:e=1  $  Humeri, upper half, medullary cavity
```

ATTACHMENT C
EXAMPLE MCNP6 INPUT FILE (continued)

```
  37     2  -1.920 -3    u=16     imp:n,p=1 $ imp:e=1   $  Humeri, lower half, cortical
  38     4  -1.108 -3    u=17     imp:n,p=1 $ imp:e=1   $  Humeri, lower half, spongiosa
  39    23  -0.980 -3    u=18     imp:n,p=1 $ imp:e=1   $  Humeri, lower half, medullary cavity
  40     2  -1.920 -3    u=19     imp:n,p=1 $ imp:e=1   $  Ulnae and radii, cortical
  41     5  -1.108 -3    u=20     imp:n,p=1 $ imp:e=1   $  Ulnae and radii, spongiosa
  42    24  -0.980 -3    u=21     imp:n,p=1 $ imp:e=1   $  Ulnae and radii, medullary cavity
  43     2  -1.920 -3    u=22     imp:n,p=1 $ imp:e=1   $  Wrists and hand bones, cortical
  44     6  -1.108 -3    u=23     imp:n,p=1 $ imp:e=1   $  Wrists and hand bones, spongiosa
  45     2  -1.920 -3    u=24     imp:n,p=1 $ imp:e=1   $  Clavicles, cortical
  46     7  -1.151 -3    u=25     imp:n,p=1 $ imp:e=1   $  Clavicles, spongiosa
  47     2  -1.920 -3    u=26     imp:n,p=1 $ imp:e=1   $  Cranium, cortical
  48     8  -1.157 -3    u=27     imp:n,p=1 $ imp:e=1   $  Cranium, spongiosa
  49     2  -1.920 -3    u=28     imp:n,p=1 $ imp:e=1   $  Femora, upper half, cortical
  50     9  -1.124 -3    u=29     imp:n,p=1 $ imp:e=1   $  Femora, upper half, spongiosa
  51    22  -0.980 -3    u=30     imp:n,p=1 $ imp:e=1   $  Femora, upper half, medullary cavity
  52     2  -1.920 -3    u=31     imp:n,p=1 $ imp:e=1   $  Femora, lower half, cortical
  53    10  -1.108 -3    u=32     imp:n,p=1 $ imp:e=1   $  Femora, lower half, spongiosa
  54    23  -0.980 -3    u=33     imp:n,p=1 $ imp:e=1   $  Femora, lower half, medullary cavity
  55     2  -1.920 -3    u=34     imp:n,p=1 $ imp:e=1   $  Tibiae, fibulae and patellae, cortical
  56    11  -1.108 -3    u=35     imp:n,p=1 $ imp:e=1   $  Tibiae, fibulae and patellae, spongiosa
  57    25  -0.980 -3    u=36     imp:n,p=1 $ imp:e=1   $  Tibiae, fibulae and patellae, medullary cavity
  58     2  -1.920 -3    u=37     imp:n,p=1 $ imp:e=1   $  Ankles and foot bones, cortical
  59    12  -1.108 -3    u=38     imp:n,p=1 $ imp:e=1   $  Ankles and foot bones, spongiosa
  60     2  -1.920 -3    u=39     imp:n,p=1 $ imp:e=1   $  Mandible, cortical
  61    13  -1.228 -3    u=40     imp:n,p=1 $ imp:e=1   $  Mandible, spongiosa
  62     2  -1.920 -3    u=41     imp:n,p=1 $ imp:e=1   $  Pelvis, cortical
  63    14  -1.123 -3    u=42     imp:n,p=1 $ imp:e=1   $  Pelvis, spongiosa
  64     2  -1.920 -3    u=43     imp:n,p=1 $ imp:e=1   $  Ribs, cortical
  65    15  -1.165 -3    u=44     imp:n,p=1 $ imp:e=1   $  Ribs, spongiosa
  66     2  -1.920 -3    u=45     imp:n,p=1 $ imp:e=1   $  Scapulae, cortical
  67    16  -1.183 -3    u=46     imp:n,p=1 $ imp:e=1   $  Scapulae, spongiosa
  68     2  -1.920 -3    u=47     imp:n,p=1 $ imp:e=1   $  Cervical spine, cortical
  69    17  -1.050 -3    u=48     imp:n,p=1 $ imp:e=1   $  Cervical spine, spongiosa
  70     2  -1.920 -3    u=49     imp:n,p=1 $ imp:e=1   $  Thoracic spine, cortical
  71    18  -1.074 -3    u=50     imp:n,p=1 $ imp:e=1   $  Thoracic spine, spongiosa
  72     2  -1.920 -3    u=51     imp:n,p=1 $ imp:e=1   $  Lumbar spine, cortical
  73    19  -1.112 -3    u=52     imp:n,p=1 $ imp:e=1   $  Lumbar spine, spongiosa
  74     2  -1.920 -3    u=53     imp:n,p=1 $ imp:e=1   $  Sacrum, cortical
  75    20  -1.031 -3    u=54     imp:n,p=1 $ imp:e=1   $  Sacrum, spongiosa
  76     2  -1.920 -3    u=55     imp:n,p=1 $ imp:e=1   $  Sternum, cortical
  77    21  -1.041 -3    u=56     imp:n,p=1 $ imp:e=1   $  Sternum, spongiosa
  78    26  -1.100 -3    u=57     imp:n,p=1 $ imp:e=1   $  Cartilage, head
  79    26  -1.100 -3    u=58     imp:n,p=1 $ imp:e=1   $  Cartilage, trunk
  80    26  -1.100 -3    u=59     imp:n,p=1 $ imp:e=1   $  Cartilage, arms
  81    26  -1.100 -3    u=60     imp:n,p=1 $ imp:e=1   $  Cartilage, legs
  82    32  -1.050 -3    u=61     imp:n,p=1 $ imp:e=1   $  Brain
  83    49  -0.950 -3    u=62     imp:n,p=1 $ imp:e=1   $  Breast, left, adipose tissue
  84    48  -1.020 -3    u=63     imp:n,p=1 $ imp:e=1   $  Breast, left, glandular tissue
  85    49  -0.950 -3    u=64     imp:n,p=1 $ imp:e=1   $  Breast, right, adipose tissue
  86    48  -1.020 -3    u=65     imp:n,p=1 $ imp:e=1   $  Breast, right, glandular tissue
  87    34  -1.050 -3    u=66     imp:n,p=1 $ imp:e=1   $  Eye lense, left
  88    34  -1.050 -3    u=67     imp:n,p=1 $ imp:e=1   $  Eye bulb, left
  89    34  -1.050 -3    u=68     imp:n,p=1 $ imp:e=1   $  Eye lense, right
  90    34  -1.050 -3    u=69     imp:n,p=1 $ imp:e=1   $  Eye bulb, right
  91    45  -1.030 -3    u=70     imp:n,p=1 $ imp:e=1   $  Gall bladder wall
  92    45  -1.030 -3    u=71     imp:n,p=1 $ imp:e=1   $  Gall bladder contents
  93    36  -1.040 -3    u=72     imp:n,p=1 $ imp:e=1   $  Stomach wall
  94    51  -1.040 -3    u=73     imp:n,p=1 $ imp:e=1   $  Stomach contents
  95    37  -1.040 -3    u=74     imp:n,p=1 $ imp:e=1   $  Small intestine wall
  96    51  -1.040 -3    u=75     imp:n,p=1 $ imp:e=1   $  Small intestine contents
  97    38  -1.040 -3    u=76     imp:n,p=1 $ imp:e=1   $  Ascending colon wall
  98    51  -1.040 -3    u=77     imp:n,p=1 $ imp:e=1   $  Ascending colon contents
  99    38  -1.040 -3    u=78     imp:n,p=1 $ imp:e=1   $  Transverse colon wall, right
 100    51  -1.040 -3    u=79     imp:n,p=1 $ imp:e=1   $  Transverse colon contents, right
 101    38  -1.040 -3    u=80     imp:n,p=1 $ imp:e=1   $  Transverse colon wall, left
 102    51  -1.040 -3    u=81     imp:n,p=1 $ imp:e=1   $  Transverse colon contents, left
 103    38  -1.040 -3    u=82     imp:n,p=1 $ imp:e=1   $  Descending colon wall
 104    51  -1.040 -3    u=83     imp:n,p=1 $ imp:e=1   $  Descending colon contents
 105    38  -1.040 -3    u=84     imp:n,p=1 $ imp:e=1   $  Sigmoid colon wall
 106    51  -1.040 -3    u=85     imp:n,p=1 $ imp:e=1   $  Sigmoid colon contents
```

ATTACHMENT C
EXAMPLE MCNP6 INPUT FILE (continued)

```
107   38  -1.040 -3   u=86   imp:n,p=1 $ imp:e=1  $  Rectum wall
108   33  -1.050 -3   u=87   imp:n,p=1 $ imp:e=1  $  Heart wall
109   28  -1.060 -3   u=88   imp:n,p=1 $ imp:e=1  $  Heart contents (blood)
110   35  -1.050 -3   u=89   imp:n,p=1 $ imp:e=1  $  Kidney, left, cortex
111   35  -1.050 -3   u=90   imp:n,p=1 $ imp:e=1  $  Kidney, left, medulla
112   35  -1.050 -3   u=91   imp:n,p=1 $ imp:e=1  $  Kidney, left, pelvis
113   35  -1.050 -3   u=92   imp:n,p=1 $ imp:e=1  $  Kidney, right, cortex
114   35  -1.050 -3   u=93   imp:n,p=1 $ imp:e=1  $  Kidney, right, medulla
115   35  -1.050 -3   u=94   imp:n,p=1 $ imp:e=1  $  Kidney, right, pelvis
116   30  -1.050 -3   u=95   imp:n,p=1 $ imp:e=1  $  Liver
117   28  -1.060 -3   u=96   imp:n,p=1 $ imp:e=1  $  Lung, left, blood
118   50  -0.382 -3   u=97   imp:n,p=1 $ imp:e=1  $  Lung, left, tissue
119   28  -1.060 -3   u=98   imp:n,p=1 $ imp:e=1  $  Lung, right, blood
120   50  -0.382 -3   u=99   imp:n,p=1 $ imp:e=1  $  Lung, right, tissue
121   47  -1.030 -3   u=100  imp:n,p=1 $ imp:e=1  $  Lymphatic nodes, extrathoracic airways
122   47  -1.030 -3   u=101  imp:n,p=1 $ imp:e=1  $  Lymphatic nodes, thoracic airways
123   47  -1.030 -3   u=102  imp:n,p=1 $ imp:e=1  $  Lymphatic nodes, head
124   47  -1.030 -3   u=103  imp:n,p=1 $ imp:e=1  $  Lymphatic nodes, trunk
125   47  -1.030 -3   u=104  imp:n,p=1 $ imp:e=1  $  Lymphatic nodes, arms
126   47  -1.030 -3   u=105  imp:n,p=1 $ imp:e=1  $  Lymphatic nodes, legs
127   29  -1.050 -3   u=106  imp:n,p=1 $ imp:e=1  $  Muscle, head
128   29  -1.050 -3   u=107  imp:n,p=1 $ imp:e=1  $  Muscle, trunk
129   29  -1.050 -3   u=108  imp:n,p=1 $ imp:e=1  $  Muscle, arms
130   29  -1.050 -3   u=109  imp:n,p=1 $ imp:e=1  $  Muscle, legs
131   44  -1.030 -3   u=110  imp:n,p=1 $ imp:e=1  $  Oesophagus
132   42  -1.040 -3   u=111  imp:n,p=1 $ imp:e=1  $  Ovary, left
133   42  -1.040 -3   u=112  imp:n,p=1 $ imp:e=1  $  Ovary, right
134   31  -1.050 -3   u=113  imp:n,p=1 $ imp:e=1  $  Pancreas
135   45  -1.030 -3   u=114  imp:n,p=1 $ imp:e=1  $  Pituitary gland
136   46  -1.030 -3   u=115  imp:n,p=1 $ imp:e=1  $  Prostate
137   49  -0.950 -3   u=116  imp:n,p=1 $ imp:e=1  $  Residual tissue, head
138   49  -0.950 -3   u=117  imp:n,p=1 $ imp:e=1  $  Residual tissue, trunk
139   49  -0.950 -3   u=118  imp:n,p=1 $ imp:e=1  $  Residual tissue, arms
140   49  -0.950 -3   u=119  imp:n,p=1 $ imp:e=1  $  Residual tissue, legs
141   45  -1.030 -3   u=120  imp:n,p=1 $ imp:e=1  $  Salivary glands, left
142   45  -1.030 -3   u=121  imp:n,p=1 $ imp:e=1  $  Salivary glands, right
143   27  -1.090 -3   u=122  imp:n,p=1 $ imp:e=1  $  Skin, head
144   27  -1.090 -3   u=123  imp:n,p=1 $ imp:e=1  $  Skin, trunk
145   27  -1.090 -3   u=124  imp:n,p=1 $ imp:e=1  $  Skin, arms
146   27  -1.090 -3   u=125  imp:n,p=1 $ imp:e=1  $  Skin, legs
147   45  -1.030 -3   u=126  imp:n,p=1 $ imp:e=1  $  Spinal cord
148   39  -1.040 -3   u=127  imp:n,p=1 $ imp:e=1  $  Spleen
149    1  -2.750 -3   u=128  imp:n,p=1 $ imp:e=1  $  Teeth
150   42  -1.040 -3   u=129  imp:n,p=1 $ imp:e=1  $  Testis, left
151   42  -1.040 -3   u=130  imp:n,p=1 $ imp:e=1  $  Testis, right
152   45  -1.030 -3   u=131  imp:n,p=1 $ imp:e=1  $  Thymus
153   40  -1.040 -3   u=132  imp:n,p=1 $ imp:e=1  $  Thyroid
154   29  -1.050 -3   u=133  imp:n,p=1 $ imp:e=1  $  Tongue (inner part)
155   45  -1.030 -3   u=134  imp:n,p=1 $ imp:e=1  $  Tonsils
156   45  -1.030 -3   u=135  imp:n,p=1 $ imp:e=1  $  Ureter, left
157   45  -1.030 -3   u=136  imp:n,p=1 $ imp:e=1  $  Ureter, right
158   41  -1.040 -3   u=137  imp:n,p=1 $ imp:e=1  $  Urinary bladder wall
159   52  -1.040 -3   u=138  imp:n,p=1 $ imp:e=1  $  Urinary bladder contents
160   46  -1.030 -3   u=139  imp:n,p=1 $ imp:e=1  $  Uterus
161   53  -0.001 -3   u=140  imp:n,p=1 $ imp:e=1  $  Air inside body
162   53  -0.001 -3   u=141  imp:n,p=1 $ imp:e=1  $  Air outside body
163   0          -3   u=256  imp:n,p=1 $ imp:e=1  $  Void Region (the zeros)
  c
  c  ==========================================================================
  c  END:  Cell/Universe Cards for ICRP-110 Adult Male Voxel Phantom
  c  ==========================================================================
  c
  c
  c  End Lattice [% Voxel Phantom %]
  c
  c  ------------------------------------------------------------------
  c  The irradiation volume
998     0     -999
              1                                       $ voxel phantom
c                300       imp:n,p=1                       $ Source Box
```

ATTACHMENT C
EXAMPLE MCNP6 INPUT FILE (continued)

```
                     imp:n,p=1                             $ No Source Box
  c
999      0     999         imp:n,p=0       $   The Great Void
  c
  c
  c  ******************* End Cell Definitions *********************************

  c  **************************************************************************
  c  |                   Surface Definition Section                           |
  c  --------------------------------------------------------------------------
  c
  c  Begin Lattice [% Voxel Phantom %]
  c    Bounding Container
1  1  rpp   0.01   54.27  0.01  27.13      0.001  177.59
  c    Lattice Unit Cell
2  1  rpp   0.000  0.2137  0.000  0.2137  0.000  0.8
  c    Lattice fill cell
3  1  so  1.0
  c  End Lattice [% Voxel Phantom %]
  c
  c
200   rpp -2.54 2.54 -0.1 0.1 -2.54 2.54   $ Dosimeter on center chest
  c
c       300 300 rpp -30 30   -201 -200  -60 60     $ Radiation Box
c       301 300 py  -200.5                         $ Radiation Surface
  c
  c
c      300 300 rpp -30 30   -201 -200  -60 60     $ Radiation Box
301    py  -200.5                         $ Radiation Surface
  c
999   so   400
  c
  c  ******************* End Surface Definitions ******************************

  c  **************************************************************************
  c  |                            Data Card Section                           |
  c  --------------------------------------------------------------------------
  c
mode n p
nps 100
  c
rand  gen=2
dbcn  48j 1      $ turn off lattice checking
  c
  c  ===== TR cards ===========================================================
  c
tr1  -27.14 -13.57 -88.8  $  Center of voxel phantom array is approx (0,0,0)
  c
  c
  c  ===========================================================================
  c  BEGIN:  TRcards for Adult Male Dosimeter Rotations
  c  ===========================================================================
  c
tr200  0 -9.6 44.5          $ Dosimeter on Center Chest
         1.000000  0.000000  0.000000  $ |
         0.000000  0.906308 -0.422618  $ | RotX(-25)
         0.000000  0.422618  0.906308  $ |
  c
tr201  5.1 -5.4 55.4        $ Dosimeter on Left Collar
         0.996195  0.078990 -0.036834  $ |
        -0.087156  0.902859 -0.421010  $ |  RotX(-25) * RotZ(5)
         0.000000  0.422618  0.906308  $ |
  c
tr202    0  -9.4 17          $ Dosimeter on center waist
  c
tr203    9.7  -10.2  42.7    $ Dosimeter on Left Chest Pocket
         0.996195  0.087156  0.000000  $ |
        -0.087156  0.996195  0.000000  $ | RotZ(5)
         0.000000  0.000000  1.000000  $ |
  c
```

ATTACHMENT C
EXAMPLE MCNP6 INPUT FILE (continued)

```
  c  ==========================================================================
  c  END:  TRcards for Adult Male Dosimeter Rotations
  c  ==========================================================================
  c
  c
  c
  c  ==========================================================================
  c  BEGIN:  TRcards for SDEF Rotations - ROT Irradiation Geometry
  c  ==========================================================================
  c
  c  tr cards for rotation of the 'door' source around
  c  the ICRP-110 Adult phantoms
  c
  c  The file simulates the ROT irradiation geometry by
  c    rotating the 'door source' at 5 deg increments
  c
  c  Data Generated by <trRotZGen_05I00S.rb>
  c    at: 2015-03-18 13:32:23 -0700
  c
  c  File:  trRotZ_05I.tr
  c
tr300   0 0 0    $ rotZ(   0)
         1.000000    0.000000    0.000000
        -0.000000    1.000000    0.000000
         0.000000    0.000000    1.000000
  c
tr301   0 0 0    $ rotZ(   5)
         0.996195    0.087156    0.000000
        -0.087156    0.996195    0.000000
         0.000000    0.000000    1.000000
  c
tr302   0 0 0    $ rotZ(  10)
         0.984808    0.173648    0.000000
        -0.173648    0.984808    0.000000
         0.000000    0.000000    1.000000
  c
tr303   0 0 0    $ rotZ(  15)
         0.965926    0.258819    0.000000
        -0.258819    0.965926    0.000000
         0.000000    0.000000    1.000000
  c
tr304   0 0 0    $ rotZ(  20)
         0.939693    0.342020    0.000000
        -0.342020    0.939693    0.000000
         0.000000    0.000000    1.000000
  c
tr305   0 0 0    $ rotZ(  25)
         0.906308    0.422618    0.000000
        -0.422618    0.906308    0.000000
         0.000000    0.000000    1.000000
  c
tr306   0 0 0    $ rotZ(  30)
         0.866025    0.500000    0.000000
        -0.500000    0.866025    0.000000
         0.000000    0.000000    1.000000
  c
tr307   0 0 0    $ rotZ(  35)
         0.819152    0.573576    0.000000
        -0.573576    0.819152    0.000000
         0.000000    0.000000    1.000000
  c
tr308   0 0 0    $ rotZ(  40)
         0.766044    0.642788    0.000000
        -0.642788    0.766044    0.000000
         0.000000    0.000000    1.000000
  c
tr309   0 0 0    $ rotZ(  45)
         0.707107    0.707107    0.000000
        -0.707107    0.707107    0.000000
         0.000000    0.000000    1.000000
```

ATTACHMENT C
EXAMPLE MCNP6 INPUT FILE (continued)

```
c
tr310   0 0 0     $ rotZ(  50)
         0.642788    0.766044    0.000000
        -0.766044    0.642788    0.000000
         0.000000    0.000000    1.000000
c
tr311   0 0 0     $ rotZ(  55)
         0.573576    0.819152    0.000000
        -0.819152    0.573576    0.000000
         0.000000    0.000000    1.000000
c
tr312   0 0 0     $ rotZ(  60)
         0.500000    0.866025    0.000000
        -0.866025    0.500000    0.000000
         0.000000    0.000000    1.000000
c
tr313   0 0 0     $ rotZ(  65)
         0.422618    0.906308    0.000000
        -0.906308    0.422618    0.000000
         0.000000    0.000000    1.000000
c
tr314   0 0 0     $ rotZ(  70)
         0.342020    0.939693    0.000000
        -0.939693    0.342020    0.000000
         0.000000    0.000000    1.000000
c
tr315   0 0 0     $ rotZ(  75)
         0.258819    0.965926    0.000000
        -0.965926    0.258819    0.000000
         0.000000    0.000000    1.000000
c
tr316   0 0 0     $ rotZ(  80)
         0.173648    0.984808    0.000000
        -0.984808    0.173648    0.000000
         0.000000    0.000000    1.000000
c
tr317   0 0 0     $ rotZ(  85)
         0.087156    0.996195    0.000000
        -0.996195    0.087156    0.000000
         0.000000    0.000000    1.000000
c
tr318   0 0 0     $ rotZ(  90)
         0.000000    1.000000    0.000000
        -1.000000    0.000000    0.000000
         0.000000    0.000000    1.000000
c
tr319   0 0 0     $ rotZ(  95)
        -0.087156    0.996195    0.000000
        -0.996195   -0.087156    0.000000
         0.000000    0.000000    1.000000
c
tr320   0 0 0     $ rotZ( 100)
        -0.173648    0.984808    0.000000
        -0.984808   -0.173648    0.000000
         0.000000    0.000000    1.000000
c
tr321   0 0 0     $ rotZ( 105)
        -0.258819    0.965926    0.000000
        -0.965926   -0.258819    0.000000
         0.000000    0.000000    1.000000
c
tr322   0 0 0     $ rotZ( 110)
        -0.342020    0.939693    0.000000
        -0.939693   -0.342020    0.000000
         0.000000    0.000000    1.000000
c
tr323   0 0 0     $ rotZ( 115)
        -0.422618    0.906308    0.000000
        -0.906308   -0.422618    0.000000
         0.000000    0.000000    1.000000
```

ATTACHMENT C
EXAMPLE MCNP6 INPUT FILE (continued)

```
c
tr324   0 0 0     $ rotZ( 120)
        -0.500000   0.866025   0.000000
        -0.866025  -0.500000   0.000000
         0.000000   0.000000   1.000000
c
tr325   0 0 0     $ rotZ( 125)
        -0.573576   0.819152   0.000000
        -0.819152  -0.573576   0.000000
         0.000000   0.000000   1.000000
c
tr326   0 0 0     $ rotZ( 130)
        -0.642788   0.766044   0.000000
        -0.766044  -0.642788   0.000000
         0.000000   0.000000   1.000000
c
tr327   0 0 0     $ rotZ( 135)
        -0.707107   0.707107   0.000000
        -0.707107  -0.707107   0.000000
         0.000000   0.000000   1.000000
c
tr328   0 0 0     $ rotZ( 140)
        -0.766044   0.642788   0.000000
        -0.642788  -0.766044   0.000000
         0.000000   0.000000   1.000000
c
tr329   0 0 0     $ rotZ( 145)
        -0.819152   0.573576   0.000000
        -0.573576  -0.819152   0.000000
         0.000000   0.000000   1.000000
c
tr330   0 0 0     $ rotZ( 150)
        -0.866025   0.500000   0.000000
        -0.500000  -0.866025   0.000000
         0.000000   0.000000   1.000000
c
tr331   0 0 0     $ rotZ( 155)
        -0.906308   0.422618   0.000000
        -0.422618  -0.906308   0.000000
         0.000000   0.000000   1.000000
c
tr332   0 0 0     $ rotZ( 160)
        -0.939693   0.342020   0.000000
        -0.342020  -0.939693   0.000000
         0.000000   0.000000   1.000000
c
tr333   0 0 0     $ rotZ( 165)
        -0.965926   0.258819   0.000000
        -0.258819  -0.965926   0.000000
         0.000000   0.000000   1.000000
c
tr334   0 0 0     $ rotZ( 170)
        -0.984808   0.173648   0.000000
        -0.173648  -0.984808   0.000000
         0.000000   0.000000   1.000000
c
tr335   0 0 0     $ rotZ( 175)
        -0.996195   0.087156   0.000000
        -0.087156  -0.996195   0.000000
         0.000000   0.000000   1.000000
c
tr336   0 0 0     $ rotZ( 180)
        -1.000000   0.000000   0.000000
        -0.000000  -1.000000   0.000000
         0.000000   0.000000   1.000000
c
tr337   0 0 0     $ rotZ( 185)
        -0.996195  -0.087156   0.000000
         0.087156  -0.996195   0.000000
         0.000000   0.000000   1.000000
```

ATTACHMENT C
EXAMPLE MCNP6 INPUT FILE (continued)

```
c
tr338   0 0 0     $ rotZ( 190)
        -0.984808   -0.173648    0.000000
         0.173648   -0.984808    0.000000
         0.000000    0.000000    1.000000
c
tr339   0 0 0     $ rotZ( 195)
        -0.965926   -0.258819    0.000000
         0.258819   -0.965926    0.000000
         0.000000    0.000000    1.000000
c
tr340   0 0 0     $ rotZ( 200)
        -0.939693   -0.342020    0.000000
         0.342020   -0.939693    0.000000
         0.000000    0.000000    1.000000
c
tr341   0 0 0     $ rotZ( 205)
        -0.906308   -0.422618    0.000000
         0.422618   -0.906308    0.000000
         0.000000    0.000000    1.000000
c
tr342   0 0 0     $ rotZ( 210)
        -0.866025   -0.500000    0.000000
         0.500000   -0.866025    0.000000
         0.000000    0.000000    1.000000
c
tr343   0 0 0     $ rotZ( 215)
        -0.819152   -0.573576    0.000000
         0.573576   -0.819152    0.000000
         0.000000    0.000000    1.000000
c
tr344   0 0 0     $ rotZ( 220)
        -0.766044   -0.642788    0.000000
         0.642788   -0.766044    0.000000
         0.000000    0.000000    1.000000
c
tr345   0 0 0     $ rotZ( 225)
        -0.707107   -0.707107    0.000000
         0.707107   -0.707107    0.000000
         0.000000    0.000000    1.000000
c
tr346   0 0 0     $ rotZ( 230)
        -0.642788   -0.766044    0.000000
         0.766044   -0.642788    0.000000
         0.000000    0.000000    1.000000
c
tr347   0 0 0     $ rotZ( 235)
        -0.573576   -0.819152    0.000000
         0.819152   -0.573576    0.000000
         0.000000    0.000000    1.000000
c
tr348   0 0 0     $ rotZ( 240)
        -0.500000   -0.866025    0.000000
         0.866025   -0.500000    0.000000
         0.000000    0.000000    1.000000
c
tr349   0 0 0     $ rotZ( 245)
        -0.422618   -0.906308    0.000000
         0.906308   -0.422618    0.000000
         0.000000    0.000000    1.000000
c
tr350   0 0 0     $ rotZ( 250)
        -0.342020   -0.939693    0.000000
         0.939693   -0.342020    0.000000
         0.000000    0.000000    1.000000
c
tr351   0 0 0     $ rotZ( 255)
        -0.258819   -0.965926    0.000000
         0.965926   -0.258819    0.000000
         0.000000    0.000000    1.000000
```

ATTACHMENT C
EXAMPLE MCNP6 INPUT FILE (continued)

```
c
tr352   0 0 0     $ rotZ( 260)
        -0.173648   -0.984808    0.000000
         0.984808   -0.173648    0.000000
         0.000000    0.000000    1.000000
c
tr353   0 0 0     $ rotZ( 265)
        -0.087156   -0.996195    0.000000
         0.996195   -0.087156    0.000000
         0.000000    0.000000    1.000000
c
tr354   0 0 0     $ rotZ( 270)
        -0.000000   -1.000000    0.000000
         1.000000   -0.000000    0.000000
         0.000000    0.000000    1.000000
c
tr355   0 0 0     $ rotZ( 275)
         0.087156   -0.996195    0.000000
         0.996195    0.087156    0.000000
         0.000000    0.000000    1.000000
c
tr356   0 0 0     $ rotZ( 280)
         0.173648   -0.984808    0.000000
         0.984808    0.173648    0.000000
         0.000000    0.000000    1.000000
c
tr357   0 0 0     $ rotZ( 285)
         0.258819   -0.965926    0.000000
         0.965926    0.258819    0.000000
         0.000000    0.000000    1.000000
c
tr358   0 0 0     $ rotZ( 290)
         0.342020   -0.939693    0.000000
         0.939693    0.342020    0.000000
         0.000000    0.000000    1.000000
c
tr359   0 0 0     $ rotZ( 295)
         0.422618   -0.906308    0.000000
         0.906308    0.422618    0.000000
         0.000000    0.000000    1.000000
c
tr360   0 0 0     $ rotZ( 300)
         0.500000   -0.866025    0.000000
         0.866025    0.500000    0.000000
         0.000000    0.000000    1.000000
c
tr361   0 0 0     $ rotZ( 305)
         0.573576   -0.819152    0.000000
         0.819152    0.573576    0.000000
         0.000000    0.000000    1.000000
c
tr362   0 0 0     $ rotZ( 310)
         0.642788   -0.766044    0.000000
         0.766044    0.642788    0.000000
         0.000000    0.000000    1.000000
c
tr363   0 0 0     $ rotZ( 315)
         0.707107   -0.707107    0.000000
         0.707107    0.707107    0.000000
         0.000000    0.000000    1.000000
c
tr364   0 0 0     $ rotZ( 320)
         0.766044   -0.642788    0.000000
         0.642788    0.766044    0.000000
         0.000000    0.000000    1.000000
c
tr365   0 0 0     $ rotZ( 325)
         0.819152   -0.573576    0.000000
         0.573576    0.819152    0.000000
         0.000000    0.000000    1.000000
```

ATTACHMENT C
EXAMPLE MCNP6 INPUT FILE (continued)

```
  c
tr366   0 0 0    $ rotZ( 330)
        0.866025  -0.500000   0.000000
        0.500000   0.866025   0.000000
        0.000000   0.000000   1.000000
  c
tr367   0 0 0    $ rotZ( 335)
        0.906308  -0.422618   0.000000
        0.422618   0.906308   0.000000
        0.000000   0.000000   1.000000
  c
tr368   0 0 0    $ rotZ( 340)
        0.939693  -0.342020   0.000000
        0.342020   0.939693   0.000000
        0.000000   0.000000   1.000000
  c
tr369   0 0 0    $ rotZ( 345)
        0.965926  -0.258819   0.000000
        0.258819   0.965926   0.000000
        0.000000   0.000000   1.000000
  c
tr370   0 0 0    $ rotZ( 350)
        0.984808  -0.173648   0.000000
        0.173648   0.984808   0.000000
        0.000000   0.000000   1.000000
  c
tr371   0 0 0    $ rotZ( 355)
        0.996195  -0.087156   0.000000
        0.087156   0.996195   0.000000
        0.000000   0.000000   1.000000
   c
   c  ===========================================================================
   c  END:  TRcards for SDEF Rotations - ROT Irradiation Geometry
   c  ===========================================================================
   c
   c
   c
   c  ~~~~~ TR cards ~~~~~~~~~~~~~~~~~~~~~~~~~~~~~~~~~~~~~~~~~~~~~~~~~~~~~~~~~~~~
   c
   c  =====  SDEF  ==============================================================
   c
   c  ==================
sdef $  Neutron Door Source
     par=n
     erg=0.3
     sur=301  tr=d5  x=d1 y=-200.5 z=d2
     nrm=1 vec=0 1 0  dir=1
     wgt=12000
   c
   c  Door Source
si1  -30 30
sp1  0  1
si2  -100 100
sp2  0 1
   c
   c  TR card info
si5 l 300 70i 371
sp5 d 1 71r
   c
   c
   c
   c  ===========================================================================
   c  BEGIN:  Material Definition Cards for ICRP-110 Adult Male Voxel Phantom
   c  ===========================================================================
   c  The material definitions include isotope information for neutron transport
   c  MT cards for lwtr S(alpha,beta) are at end of the definition
   c
   c  File:  ICRP110_AM_mCard.N.mtrl
   c
   c
```

ATTACHMENT C
EXAMPLE MCNP6 INPUT FILE (continued)

```
  c
m1    $  Teeth
       1001  -2.2 $  H
       6000  -9.5 $  C
       7014  -2.9 $  N
       8016 -42.1 $  O
      12000  -0.7 $ Mg
      15031 -13.7 $  P
      20000 -28.9 $ Ca
  c
m2  $   Mineral bone
       1001  -3.6 $  H
       6000 -15.9 $  C
       7014  -4.2 $  N
       8016 -44.8 $  O
      11023  -0.3 $ Na
      12000  -0.2 $ Mg
      15031  -9.4 $  P
      16000  -0.3 $  S
      20000 -21.3 $ Ca
  c
m3     $     Humeri, upper half, spongiosa
       1001  -8.5 $  H
       6000 -28.8 $  C
       7014  -2.6 $  N
       8016 -49.8 $  O
      11023  -0.2 $ Na
      12000  -0.1 $ Mg
      15031  -3.3 $  P
      16000  -0.4 $  S
      17000  -0.2 $ Cl
      20000  -6.1 $ Ca
  c
m4    $  Humeri, lower half, spongiosa
       1001  -9.7 $  H
       6000 -43.9 $  C
       7014  -1.7 $  N
       8016 -38.1 $  O
      11023  -0.2 $ N
      15031  -2.1 $  P
      16000  -0.3 $  S
      17000  -0.1 $ Cl
      20000  -3.9 $ Ca
  c
m5    $  Lower arm bones, spongiosa
       1001  -9.7 $  H
       6000 -43.9 $  C
       7014  -1.7 $  N
       8016 -38.1 $  O
      11023  -0.2 $ Na
      15031  -2.1 $  P
      16000  -0.3 $  S
      17000  -0.1 $ Cl
      20000  -3.9 $ Ca
  c
m6    $  Hand bones, spongiosa
       1001  -9.7 $  H
       6000 -43.9 $  C
       7014  -1.7 $  N
       8016 -38.1 $  O
      11023  -0.2 $ Na
      15031  -2.1 $  P
      16000  -0.3 $  S
      17000  -0.1 $ Cl
      20000  -3.9 $ Ca
  c
m7    $  Clavicles, spongiosa
       1001  -9.1 $  H
       6000 -34.8 $  C
       7014  -2.4 $  N
```

ATTACHMENT C
EXAMPLE MCNP6 INPUT FILE (continued)

```
        8016 -45.7 $  O
       11023  -0.2 $ Na
       15031  -2.6 $  P
       16000  -0.3 $  S
       17000  -0.1 $ Cl
       20000  -4.8 $ Ca
  c
m8    $  Cranium, spongiosa
        1001  -9.0 $  H
        6000 -33.5 $  C
        7014  -2.5 $  N
        8016 -46.7 $  O
       11023  -0.2 $ Na
       15031  -2.6 $  P
       16000  -0.3 $  S
       17000  -0.2 $ Cl
       19000  -0.1 $  K
       20000  -4.9 $ Ca
  c
m9    $  Femora, upper half, spongiosa
        1001  -9.4 $  H
        6000 -38.5 $  C
        7014  -2.2 $  N
        8016 -43.0 $  O
       11023  -0.2 $ Na
       15031  -2.2 $  P
       16000  -0.3 $  S
       17000  -0.1 $ Cl
       20000  -4.1 $ Ca
  c
m10   $  Femora, lower half, spongiosa
        1001  -9.7 $  H
        6000 -43.9 $  C
        7014  -1.7 $  N
        8016 -38.1 $  O
       11023  -0.2 $ Na
       15031  -2.1 $  P
       16000  -0.3 $  S
       17000  -0.1 $ Cl
       20000  -3.9 $ Ca
  c
m11   $  Lower leg bones, spongiosa
        1001  -9.7 $  H
        6000 -43.9 $  C
        7014  -1.7 $  N
        8016 -38.1 $  O
       11023  -0.2 $ Na
       15031  -2.1 $  P
       16000  -0.3 $  S
       17000  -0.1 $ Cl
       20000  -3.9 $ Ca
  c
m12   $  Foot bones, spongiosa
        1001  -9.7 $  H
        6000 -43.9 $  C
        7014  -1.7 $  N
        8016 -38.1 $  O
       11023  -0.2 $ Na
       15031  -2.1 $  P
       16000  -0.3 $  S
       17000  -0.1 $ Cl
       20000  -3.9 $ Ca
  c
m13   $  Mandible, spongiosa
        1001  -8.3 $  H
        6000 -26.6 $  C
        7014  -2.7 $  N
        8016 -51.1 $  O
       11023  -0.3 $ Na
       12000  -0.1 $ Mg
```

ATTACHMENT C
EXAMPLE MCNP6 INPUT FILE (continued)

```
       15031  -3.6 $  P
       16000  -0.4 $  S
       17000  -0.2 $ Cl
       20000  -6.7 $ Ca
  c
m14   $  Pelvis, spongiosa
        1001  -9.4 $  H
        6000 -36.0 $  C
        7014  -2.5 $  N
        8016 -45.4 $  O
       11023  -0.2 $ Na
       15031  -2.1 $  P
       16000  -0.3 $  S
       17000  -0.2 $ Cl
       19000  -0.1 $  K
       20000  -3.8 $ Ca
  c
m15   $  Ribs, spongiosa
        1001  -8.9 $  H
        6000 -29.2 $  C
        7014  -2.9 $  N
        8016 -50.7 $  O
       11023  -0.2 $ Na
       15031  -2.6 $  P
       16000  -0.4 $  S
       17000  -0.2 $ Cl
       19000  -0.1 $  K
       20000  -4.8 $ Ca
  c
m16   $  Scapulae, spongiosa
        1001  -8.7 $  H
        6000 -30.9 $  C
        7014  -2.6 $  N
        8016 -48.3 $  O
       11023  -0.2 $ Na
       12000  -0.1 $ Mg
       15031  -3.0 $  P
       16000  -0.4 $  S
       17000  -0.2 $ Cl
       20000  -5.6 $ Ca
  c
m17   $  Cervical spine, spongiosa
        1001 -10.3 $  H
        6000 -40.0 $  C
        7014  -2.7 $  N
        8016 -44.4 $  O
       11023  -0.1 $ Na
       15031  -0.7 $  P
       16000  -0.2 $  S
       17000  -0.2 $ Cl
       19000  -0.1 $  K
       20000  -1.2 $ Ca
     c 26000  -0.1 $ Fe
       26054  -0.000056
       26056  -0.000919
       26057  -0.000022
       26058  -0.000003
  c
m18   $  Thoracic spine, spongiosa
        1001  -9.9 $  H
        6000 -37.6 $  C
        7014  -2.7 $  N
        8016 -45.9 $  O
       11023  -0.1 $ Na
       15031  -1.2 $  P
       16000  -0.2 $  S
       17000  -0.2 $ Cl
       19000  -0.1 $  K
       20000  -2.0 $ Ca
     c 26000  -0.1 $ Fe
```

ATTACHMENT C
EXAMPLE MCNP6 INPUT FILE (continued)

```
       26054  -0.000056
       26056  -0.000919
       26057  -0.000022
       26058  -0.000003
   c
m19  $  Lumbar spine, spongiosa
        1001  -9.5 $  H
        6000 -34.0 $  C
        7014  -2.8 $  N
        8016 -48.0 $  O
       11023  -0.1 $ Na
       15031  -1.8 $  P
       16000  -0.3 $  S
       17000  -0.2 $ Cl
       19000  -0.1 $  K
       20000  -3.2 $ Ca
   c
m20  $  Sacrum, spongiosa
        1001 -10.5 $  H
        6000 -41.9 $  C
        7014  -2.7 $  N
        8016 -43.2 $  O
       11023  -0.1 $ Na
       15031  -0.4 $  P
       16000  -0.2 $  S
       17000  -0.2 $ Cl
       19000  -0.1 $  K
       20000  -0.6 $ Ca
     c 26000  -0.1 $ Fe
       26054  -0.000056
       26056  -0.000919
       26057  -0.000022
       26058  -0.000003
   c
m21  $  Sternum, spongiosa
        1001 -10.4 $  H
        6000 -40.9 $  C
        7014  -2.7 $  N
        8016 -43.8 $  O
       11023  -0.1 $ Na
       15031  -0.6 $  P
       16000  -0.2 $  S
       17000  -0.2 $ Cl
       19000  -0.1 $  K
       20000  -0.9 $ Ca
     c 26000  -0.1 $ Fe
       26054  -0.000056
       26056  -0.000919
       26057  -0.000022
       26058  -0.000003
   c
m22  $  Humeri and femora, upper halves, medullary cavity
        1001 -11.5 $  H
        6000 -63.6 $  C
        7014  -0.7 $  N
        8016 -23.9 $  O
       11023  -0.1 $ Na
       16000  -0.1 $  S
       17000  -0.1 $ Cl
   c
m23  $  Humeri and femora, lower halves, medullary cavity
        1001 -11.5 $  H
        6000 -63.6 $  C
        7014  -0.7 $  N
        8016 -23.9 $  O
       11023  -0.1 $ Na
       16000  -0.1 $  S
       17000  -0.1 $ Cl
   c
m24  $  Lower arm bones, medullary cavity
```

ATTACHMENT C
EXAMPLE MCNP6 INPUT FILE (continued)

```
        1001 -11.5 $  H
        6000 -63.6 $  C
        7014  -0.7 $  N
        8016 -23.9 $  O
       11023  -0.1 $ Na
       16000  -0.1 $  S
       17000  -0.1 $ Cl
  c
m25  $  Lower leg bones, medullary cavity
        1001 -11.5 $  H
        6000 -63.6 $  C
        7014  -0.7 $  N
        8016 -23.9 $  O
       11023  -0.1 $ Na
       16000  -0.1 $  S
       17000  -0.1 $ Cl
  c
m26  $  Cartilage
        1001  -9.6 $  H
        6000  -9.9 $  C
        7014  -2.2 $  N
        8016 -74.4 $  O
       11023  -0.5 $ Na
       15031  -2.2 $  P
       16000  -0.9 $  S
       17000  -0.3 $ Cl
  c
m27  $  Skin
        1001 -10.0 $  H
        6000 -19.9 $  C
        7014  -4.2 $  N
        8016 -65.0 $  O
       11023  -0.2 $ Na
       15031  -0.1 $  P
       16000  -0.2 $  S
       17000  -0.3 $ Cl
       19000  -0.1 $  K
  c
m28  $  Blood
        1001 -10.2 $  H
        6000 -11.0 $  C
        7014  -3.3 $  N
        8016 -74.5 $  O
       11023  -0.1 $ Na
       15031  -0.1 $  P
       16000  -0.2 $  S
       17000  -0.3 $ Cl
       19000  -0.2 $  K
     c 26000  -0.1 $ Fe
       26054  -0.000056
       26056  -0.000919
       26057  -0.000022
       26058  -0.000003
  c
m29  $  Muscle tissue
        1001 -10.2 $  H
        6000 -14.2 $  C
        7014  -3.4 $  N
        8016 -71.1 $  O
       11023  -0.1 $ Na
       15031  -0.2 $  P
       16000  -0.3 $  S
       17000  -0.1 $ Cl
       19000  -0.4 $  K
  c
m30  $  Liver
        1001 -10.2 $  H
        6000 -13.0 $  C
        7014  -3.1 $  N
        8016 -72.5 $  O
```

ATTACHMENT C
EXAMPLE MCNP6 INPUT FILE (continued)

```
        11023  -0.2 $ Na
        15031  -0.2 $  P
        16000  -0.3 $  S
        17000  -0.2 $ Cl
        19000  -0.3 $  K
c
m31  $  Pancreas
         1001 -10.5 $  H
         6000 -15.5 $  C
         7014  -2.5 $  N
         8016 -70.6 $  O
        11023  -0.2 $ Na
        16000  -0.1 $  S
        17000  -0.2 $ Cl
        19000  -0.2 $  K
c
m32  $  Brain
         1001 -10.7 $  H
         6000 -14.3 $  C
         7014  -2.3 $  N
         8016 -71.3 $  O
        11023  -0.2 $ Na
        15031  -0.4 $  P
        16000  -0.2 $  S
        17000  -0.3 $ Cl
        19000  -0.3 $  K
c
m33  $  Heart
         1001 -10.4 $  H
         6000 -13.8 $  C
         7014  -2.9 $  N
         8016 -71.9 $  O
        11023  -0.1 $ Na
        15031  -0.2 $  P
        16000  -0.2 $  S
        17000  -0.2 $ Cl
        19000  -0.3 $  K
c
m34  $  Eyes
         1001  -9.7 $  H
         6000 -18.1 $  C
         7014  -5.3 $  N
         8016 -66.3 $  O
        11023  -0.1 $ Na
        15031  -0.1 $  P
        16000  -0.3 $  S
        17000  -0.1 $ Cl
c
m35  $  Kidneys
         1001 -10.3 $  H
         6000 -12.4 $  C
         7014  -3.1 $  N
         8016 -73.1 $  O
        11023  -0.2 $ Na
        15031  -0.2 $  P
        16000  -0.2 $  S
        17000  -0.2 $ Cl
        19000  -0.2 $  K
        20000  -0.1 $ Ca
c
m36  $  Stomach
         1001 -10.5 $  H
         6000 -11.4 $  C
         7014  -2.5 $  N
         8016 -75.0 $  O
        11023  -0.1 $ Na
        15031  -0.1 $  P
        16000  -0.1 $  S
        17000  -0.2 $ Cl
        19000  -0.1 $  K
```

ATTACHMENT C
EXAMPLE MCNP6 INPUT FILE (continued)

```
c
m37  $  Small intestine
       1001 -10.5 $  H
       6000 -11.3 $  C
       7014  -2.6 $  N
       8016 -75.0 $  O
      11023  -0.1 $ Na
      15031  -0.1 $  P
      16000  -0.1 $  S
      17000  -0.2 $ Cl
      19000  -0.1 $  K
c
m38  $  Large intestine
       1001 -10.5 $  H
       6000 -11.3 $  C
       7014  -2.6 $  N
       8016 -75.0 $  O
      11023  -0.1 $ Na
      15031  -0.1 $  P
      16000  -0.1 $  S
      17000  -0.2 $ Cl
      19000  -0.1 $  K
c
m39  $  Spleen
       1001 -10.2 $  H
       6000 -11.1 $  C
       7014  -3.3 $  N
       8016 -74.3 $  O
      11023  -0.1 $ Na
      15031  -0.2 $  P
      16000  -0.2 $  S
      17000  -0.3 $ Cl
      19000  -0.2 $  K
    c 26000  -0.1 $ Fe
      26054  -0.000056
      26056  -0.000919
      26057  -0.000022
      26058  -0.000003
c
m40  $  Thyroid
       1001 -10.4 $  H
       6000 -11.7 $  C
       7014  -2.6 $  N
       8016 -74.5 $  O
      11023  -0.2 $ Na
      15031  -0.1 $  P
      16000  -0.1 $  S
      17000  -0.2 $ Cl
      19000  -0.1 $  K
      53127  -0.1 $  I
c
m41  $  Urinary bladder
       1001 -10.5 $  H
       6000  -9.6 $  C
       7014  -2.6 $  N
       8016 -76.1 $  O
      11023  -0.2 $ Na
      15031  -0.2 $  P
      16000  -0.2 $  S
      17000  -0.3 $ Cl
      19000  -0.3 $  K
c
m42  $  Testes
       1001 -10.6 $  H
       6000 -10.0 $  C
       7014  -2.1 $  N
       8016 -76.4 $  O
      11023  -0.2 $ Na
      15031  -0.1 $  P
      16000  -0.2 $  S
```

ATTACHMENT C
EXAMPLE MCNP6 INPUT FILE (continued)

```
      17000  -0.2 $ Cl
      19000  -0.2 $  K
  c
m43  $  Adrenals
       1001 -10.4 $  H
       6000 -22.1 $  C
       7014  -2.8 $  N
       8016 -63.7 $  O
      11023  -0.1 $ Na
      15031  -0.2 $  P
      16000  -0.3 $  S
      17000  -0.2 $ Cl
      19000  -0.2 $  K
  c
m44  $  Oesophagus
       1001 -10.4 $  H
       6000 -21.3 $  C
       7014  -2.9 $  N
       8016 -64.4 $  O
      11023  -0.1 $ Na
      15031  -0.2 $  P
      16000  -0.3 $  S
      17000  -0.2 $ Cl
      19000  -0.2 $  K
  c
m45  $  Gallbladder, Pituitary gland, Trachea, Thymus, Tonsils, Ureters, ...
       1001 -10.4 $  H
       6000 -23.1 $  C
       7014  -2.8 $  N
       8016 -62.7 $  O
      11023  -0.1 $ Na
      15031  -0.2 $  P
      16000  -0.3 $  S
      17000  -0.2 $ Cl
      19000  -0.2 $  K
  c
m46  $  Prostate
       1001 -10.4 $  H
       6000 -23.1 $  C
       7014  -2.8 $  N
       8016 -62.7 $  O
      11023  -0.1 $ Na
      15031  -0.2 $  P
      16000  -0.3 $  S
      17000  -0.2 $ Cl
      19000  -0.2 $  K
  c
m47  $  Lymph
       1001 -10.8 $  H
       6000  -4.2 $  C
       7014  -1.1 $  N
       8016 -83.1 $  O
      11023  -0.3 $ Na
      16000  -0.1 $  S
      17000  -0.4 $ Cl
  c
m48  $  Breast (mammary gland)
       1001 -11.2 $  H
       6000 -51.6 $  C
       7014  -1.1 $  N
       8016 -35.8 $  O
      11023  -0.1 $ Na
      16000  -0.1 $  S
      17000  -0.1 $ Cl
  c
m49  $  Adipose tissue
       1001 -11.4 $  H
       6000 -58.8 $  C
       7014  -0.8 $  N
       8016 -28.7 $  O
```

ATTACHMENT C
EXAMPLE MCNP6 INPUT FILE (continued)

```
      11023  -0.1 $ Na
      16000  -0.1 $  S
      17000  -0.1 $ Cl
  c
m50  $  Lung tissue (compressed lungs)
       1001 -10.3 $  H
       6000 -10.7 $  C
       7014  -3.2 $  N
       8016 -74.6 $  O
      11023  -0.2 $ Na
      15031  -0.2 $  P
      16000  -0.3 $  S
      17000  -0.3 $ Cl
      19000  -0.2 $  K
  c
m51  $  Gastro-intestinal tract - contents
       1001 -10.0 $  H
       6000 -22.2 $  C
       7014  -2.2 $  N
       8016 -64.4 $  O
      11023  -0.1 $ Na
      15031  -0.2 $  P
      16000  -0.3 $  S
      17000  -0.1 $ Cl
      19000  -0.4 $  K
      20000  -0.1 $ Ca
  c
m52  $  Urine
       1001 -10.7 $  H
       6000  -0.3 $  C
       7014  -1.0 $  N
       8016 -87.3 $  O
      11023  -0.4 $ Na
      15031  -0.1 $  P
      19000  -0.2 $  K
  c
m53  $  Air
       7014 -80.0 $  N
       8016 -20.0 $  O
  c  ~~~~~~~~~~~~~~~~~~~~~~~~~~~~~~~~~~~~~~~~~~~~~~~~~~~~~~~~~~~~~~~~~~~~~~~~~~~~
  c  S(alpha,beta) treatment
  c
mt1   lwtr.10t $  Teeth
mt2   lwtr.10t $  Mineral bone
mt3   lwtr.10t $  Humeri, upper half, spongiosa
mt4   lwtr.10t $  Humeri, lower half, spongiosa
mt5   lwtr.10t $  Lower arm bones, spongiosa
mt6   lwtr.10t $  Hand bones, spongiosa
mt7   lwtr.10t $  Clavicles, spongiosa
mt8   lwtr.10t $  Cranium, spongiosa
mt9   lwtr.10t $  Femora, upper half, spongiosa
mt10  lwtr.10t $  Femora, lower half, spongiosa
mt11  lwtr.10t $  Lower leg bones, spongiosa
mt12  lwtr.10t $  Foot bones, spongiosa
mt13  lwtr.10t $  Mandible, spongiosa
mt14  lwtr.10t $  Pelvis, spongiosa
mt15  lwtr.10t $  Ribs, spongiosa
mt16  lwtr.10t $  Scapulae, spongiosa
mt17  lwtr.10t $  Cervical spine, spongiosa
mt18  lwtr.10t $  Thoracic spine, spongiosa
mt19  lwtr.10t $  Lumbar spine, spongiosa
mt20  lwtr.10t $  Sacrum, spongiosa
mt21  lwtr.10t $  Sternum, spongiosa
mt22  lwtr.10t $  Humeri and femora, upper halves, medullary cavity
mt23  lwtr.10t $  Humeri and femora, lower halves, medullary cavity
mt24  lwtr.10t $  Lower arm bones, medullary cavity
mt25  lwtr.10t $  Lower leg bones, medullary cavity
mt26  lwtr.10t $  Cartilage
mt27  lwtr.10t $  Skin
mt28  lwtr.10t $  Blood
```

ATTACHMENT C
EXAMPLE MCNP6 INPUT FILE (continued)

```
mt29  lwtr.10t $  Muscle tissue
mt30  lwtr.10t $  Liver
mt31  lwtr.10t $  Pancreas
mt32  lwtr.10t $  Brain
mt33  lwtr.10t $  Heart
mt34  lwtr.10t $  Eyes
mt35  lwtr.10t $  Kidneys
mt36  lwtr.10t $  Stomach
mt37  lwtr.10t $  Small intestine
mt38  lwtr.10t $  Large intestine
mt39  lwtr.10t $  Spleen
mt40  lwtr.10t $  Thyroid
mt41  lwtr.10t $  Urinary bladder
mt42  lwtr.10t $  Testes
mt43  lwtr.10t $  Adrenals
mt44  lwtr.10t $  Oesophagus
mt45  lwtr.10t $  Gallbladder, Pituitary gland, Trachea, Thymus, Tonsils, Ureters, ...
mt46  lwtr.10t $  Prostate
mt47  lwtr.10t $  Lymph
mt48  lwtr.10t $  Breast (mammary gland)
mt49  lwtr.10t $  Adipose tissue
mt50  lwtr.10t $  Lung tissue (compressed lungs)
mt51  lwtr.10t $  Gastro-intestinal tract - contents
mt52  lwtr.10t $  Urine
  c
  c
  c  ========================================================================
  c  END:  Material Definition Cards for ICRP-110 Adult Male Voxel Phantom
  c  ========================================================================
  c
  c
  c
  c
  c  =====  TALLY  ==========================================================
  c
  c  Dosimeter Doses
  c
  c
  c  Energies from ICRP-74 Table A.42 with additions from ICRP-116 Tables C.*
e4    0.00     1.00E-09 1.00E-08 2.50E-08 2.53E-08 1.00E-07 2.00E-07 5.00E-07
      1.00E-06 2.00E-06 5.00E-06 1.00E-05 2.00E-05 5.00E-05 1.00E-04 2.00E-04
      5.00E-04 1.00E-03 2.00E-03 5.00E-03 1.00E-02 2.00E-02 3.00E-02 5.00E-02
      7.00E-02 1.00E-01 1.50E-01 2.00E-01 3.00E-01 5.00E-01 7.00E-01 9.00E-01
      1.00E+00 1.20E+00 1.50E+00 2.00E+00 3.00E+00 4.00E+00 5.00E+00 6.00E+00
      7.00E+00 8.00E+00 9.00E+00 1.00E+01 1.20E+01 1.40E+01 1.50E+01 1.60E+01
      1.80E+01 2.00E+01 2.10E+01 3.00E+01 5.00E+01 7.50E+01 1.00E+02 1.25E+02
      1.30E+02 1.50E+02 1.75E+02 1.80E+02 2.01E+02
  c
  c  Energies from ICRP-74 Table A.42 with additions from ICRP-116 Tables C.*
e14   0.00     1.00E-09 1.00E-08 2.50E-08 2.53E-08 1.00E-07 2.00E-07 5.00E-07
      1.00E-06 2.00E-06 5.00E-06 1.00E-05 2.00E-05 5.00E-05 1.00E-04 2.00E-04
      5.00E-04 1.00E-03 2.00E-03 5.00E-03 1.00E-02 2.00E-02 3.00E-02 5.00E-02
      7.00E-02 1.00E-01 1.50E-01 2.00E-01 3.00E-01 5.00E-01 7.00E-01 9.00E-01
      1.00E+00 1.20E+00 1.50E+00 2.00E+00 3.00E+00 4.00E+00 5.00E+00 6.00E+00
      7.00E+00 8.00E+00 9.00E+00 1.00E+01 1.20E+01 1.40E+01 1.50E+01 1.60E+01
      1.80E+01 2.00E+01 2.10E+01 3.00E+01 5.00E+01 7.50E+01 1.00E+02 1.25E+02
      1.30E+02 1.50E+02 1.75E+02 1.80E+02 2.01E+02
  c
  c
  c  Dosimeter Fluence
f4:n  200  201  202  203
  c
  c
  c  Dosimeter Hp(10)
f14:n  200  201  202  203
  c
  c  Fluence to Hp(10) Conversion Factors
  c
  c  Hp(10) for slab @ 0 deg (pSv cm2)  ICRP-74; Table A.42
  c   E(MeV)
```

ATTACHMENT C
EXAMPLE MCNP6 INPUT FILE (continued)

```
de14  1.00E-09 1.00E-08 2.53E-08 1.00E-07 2.00E-07 5.00E-07 1.00E-06 2.00E-06
      5.00E-06 1.00E-05 2.00E-05 5.00E-05 1.00E-04 2.00E-04 5.00E-04 1.00E-03
      2.00E-03 5.00E-03 1.00E-02 2.00E-02 3.00E-02 5.00E-02 7.00E-02 1.00E-01
      1.50E-01 2.00E-01 3.00E-01 5.00E-01 7.00E-01 9.00E-01 1.00E+00 1.20E+00
      2.00E+00 3.00E+00 4.00E+00 5.00E+00 6.00E+00 7.00E+00 8.00E+00 9.00E+00
      1.00E+01 1.20E+01 1.40E+01 1.50E+01 1.60E+01 1.80E+01 2.00E+01
  c   Hp(10) for slab @ 0 deg (pSv cm2)
df14    8.19     9.97   11.4      12.6      13.5      14.2      14.4      14.3
       13.8     13.2    12.4      11.2      10.3       9.84      9.34      8.78
        8.72     9.36   11.2      17.1      24.9      39.0      59.0      90.6
      139      180     246       335       386       414       422       433
      442      431     422       420       423       432       445       461
      480      517     550       564       576       595       600
  c
  c
  c
  c  Organ Doses
  c    +F6: Path Length Estimator of Dose  (MeV/g)
  c                   Lung
  c    LLung(B)   LLung(T)   RLung(B)   RLung(T)
+f6   (117<7<8)  (118<7<8)  (119<7<8)  (120<7<8)
sd6    79.00       474.25     71.53      575.84
  c                      Kidney
  c    LCortex    LMedulla   LPelvis    RCortex    RMedulla   RPelvis
+f16  (110<7<8) (111<7<8)  (112<7<8)  (113<7<8)  (114<7<8)  (115<7<8)
sd16   107.10     38.25       7.63       109.90    39.24       7.86
  c                   Single Cell Organs
  c    Brain     Heart Wall Liver     Pancreas  Thyroid   UB Wall
+f26  (82<7<8)  (108<7<8)  (116<7<8) (134<7<8) (153<7<8) (158<7<8)
sd26    1449.81   329.94     1799.78   139.98    19.99     50.08
  c
  c
  c  Organ Doses
  c    F6:n,p Path Length Estimator of Dose  (MeV/g)
  c                   Lung
  c    LLung(B)   LLung(T)   RLung(B)   RLung(T)
f106:n,p    (117<7<8)  (118<7<8)  (119<7<8)  (120<7<8)
sd106    79.00       474.25     71.53      575.84
  c                      Kidney
  c    LCortex    LMedulla   LPelvis    RCortex    RMedulla   RPelvis
f116:n,p  (110<7<8) (111<7<8)  (112<7<8)  (113<7<8)  (114<7<8)  (115<7<8)
sd116   107.10     38.25       7.63       109.90    39.24       7.86
  c                   Single Cell Organs
  c    Brain     Heart Wall Liver     Pancreas  Thyroid   UB Wall
f126:n,p  (82<7<8)  (108<7<8)  (116<7<8) (134<7<8) (153<7<8) (158<7<8)
sd126    1449.81   329.94     1799.78   139.98    19.99     50.08
  c
  c
  c  ~~~~~  TALLY  ~~~~~~~~~~~~~~~~~~~~~~~~~~~~~~~~~~~~~~~~~~~~~~~~~~~~~~~~~~~~~~~~
  c
  c
  c  =====  Peripheral Cards  ==================================================
  c
prdmp  j j 1 4        $  Request MCTAL file and 4 dumps to RUNTPE
  c
  c  ~~~~~  Peripheral Cards  ~~~~~~~~~~~~~~~~~~~~~~~~~~~~~~~~~~~~~~~~~~~~~~~~~~
  c
  c
  c
  c  ******************* End Data Card Section *********************************
```

ATTACHMENT D
RESULTS OF REFERENCE CALCULATIONS

LIST OF FIGURES

FIGURES **TITLE** **PAGE**

D-1 Relative differences between ICRP-evaluated DCCs and ORAU Team-calculated DCCs, adult female reference organs, monoenergetic neutrons, AP geometry 57
D-2 Relative differences between ICRP-evaluated DCCs and ORAU Team-calculated DCCs, adult male reference organs, monoenergetic neutrons, AP geometry 57
D-3 Relative differences between ICRP-evaluated DCCs and ORAU Team-calculated DCCs, adult female reference organs, monoenergetic neutrons, ROT geometry.............................. 58
D-4 Relative differences between ICRP-evaluated DCCs and ORAU Team-calculated DCCs, adult male reference organs, monoenergetic neutrons, ROT geometry................................. 58
D-5 Relative differences between ICRP-evaluated DCCs and ORAU Team-calculated DCCs, adult female reference organs, monoenergetic neutrons, ISO geometry 59
D-6 Relative differences between ICRP-evaluated DCCs and ORAU Team-calculated DCCs, adult male reference organs, monoenergetic neutrons, ISO geometry 59
D-7 Relative differences between ICRP-evaluated DCCs and ORAU Team-calculated DCCs, adult female reference organs, monoenergetic photons, AP geometry.................................. 60
D-8 Relative differences between ICRP-evaluated DCCs and ORAU Team-calculated DCCs, adult male reference organs, monoenergetic photons, AP geometry 60
D-9 Relative differences between ICRP-evaluated DCCs and ORAU Team-calculated DCCs, adult female reference organs, monoenergetic photons, ROT geometry............................... 61
D-10 Relative differences between ICRP-evaluated DCCs and ORAU Team-calculated DCCs, adult male reference organs, monoenergetic photons, ROT geometry.................................. 61
D-11 Relative differences between ICRP-evaluated DCCs and ORAU Team-calculated DCCs, adult female reference organs, monoenergetic photons, ISO geometry 62
D-12 Relative differences between ICRP-evaluated DCCs and ORAU Team-calculated DCCs, adult male reference organs, monoenergetic photons, ISO geometry 62
D-13 Comparison between ICRP-evaluated DCCs and ORAU Team-calculated DCCs, adult female and male urinary bladder wall, monoenergetic neutrons, AP geometry....................... 63

ATTACHMENT D
RESULTS OF REFERENCE CALCULATIONS (continued)

Figures D-1 to D-13 show the results of the benchmarking calculations that were described in Sections 2.4 and 3.1. The figures compare the organ DCCs calculated with MCNP6.1 for this report to those in ICRP Publication 116 (ICRP 2010). The figures show the relative difference between the two sets of dose calculations. The figures show the results for irradiation of the adult male and adult female voxel phantoms by neutrons and photons in the AP, ROT, and ISO irradiation geometries.

The absorbed DCCs that were calculated for benchmarking were obtained by applying a cubic spline smoothing function to the calculated data to obtain a smooth curve of the DCCs as a function of neutron or photon energy, as applicable. In similarity to ICRP, the DCCs at specified energy points were evaluated using the smoothed data curve.

For the MCNP6.1 calculated data, the R (R Core Team 2014) function “smooth.spline” was used to compute the cubic spline object from log-log transformed data and the function “predict.smooth.spline” was used to evaluate the fitted data. The energy-specific DCCs calculated for this report were compared with the evaluated DCCs calculated by ICRP (2010).

The figures in this attachment provide a subjective view of how well the DCCs calculated for the benchmarking organs agree with the DCCs in ICRP Publication 116 (ICRP 2010). In all figures, the notation “ICRP” refers to the DCCs tabulated in Publication 116, and the notation “ORAUT” refers to the DCCs calculated for this report. The good agreement between the ICRP DCCs and the ORAUT DCCs indicates that the ORAUT implementations of the ICRP voxel phantoms and the irradiation geometries are correct.

Figures D-1 through D-12 show the pointwise relative difference between the ICRP and ORAUT DCCs for all eight reference organs. The relative difference, *RD*, between ICRP and ORAUT absorbed DCCs was calculated using Equation D-1:

$$RD = \frac{\left(DCC_{\text{ORAUT}} - DCC_{\text{ICRP}}\right)}{DCC_{\text{ICRP}}} \qquad \text{D-1}$$

Where DCC_{ICRP} is the particle and energy-specific DCC calculated by the ICRP and DCC_{ORAUT} is the corresponding particle and energy-specific DCC calculated for this report.

Figures D-1 through D-6 show the results for incident neutrons while Figures D-7 through D-12 show the results for incident photons.

Referring to Figures D-1 through D-6, the ORAUT DCCs appear to be biased high for 20 MeV incident neutrons. This apparent bias is caused by how the cubic spline smoother calculates smoothed data at the endpoints of the data. The ORAUT data terminate at 20 MeV while the ICRP data continue on to 10 GeV and are thus more constrained than are the ORAUT data.

Referring to Figures D-1, D-3 and D-5, the ORAUT DCCs appear to be biased high in the 0.005 to 0.03 MeV neutron energy region. Figure D-13 compares the ORAUT and ICRP DCCs for the urinary bladder wall, the organ that shows maximal bias of the ORAUT calculations, for both the female and male phantoms. This figure shows that the the ORAUT and ICRP DCCs for the adult male phantom agree well at all energies but that for the adult female phantom, in the energy region defined above, there is divergence between the ORAUT and ICRP DCCs. Although not shown here, additional plots, similar to Fig D-13 and plots of the total neutron cross section for urinary bladder wall tissue, which is identical for the female and male phantoms, indicate that the ICRP DCCs are slightly smaller than the

ATTACHMENT D
RESULTS OF REFERENCE CALCULATIONS (continued)

ORAUT DCCs and the difference occurs in the region of the total neutron cross section plot where the cross section rolls-off from a level region. The cause of the bias has not been determined but has been noted, investigated, and is evaluated to be small and does not appear to be due to errors in modeling. The cause of the apparent bias will be investigated when it becomes important to calculate radiation doses to organs.

Referring to Figure D-13, a vertical line denotes the DCCs that are calculated when the phantoms are irradiated by 1-MeV neutrons. The plotting symbol shows the DCC calculated using MCNP6.1, while the solid line shows the smoothed data. A similar deviation at 1 MeV is seen in Publication 116 Annex I for the ICRP calculations (ICRP 2010). The deviation is a reduction in the DCC due to a resonance peak in the neutron cross section of ^{16}O at 1 MeV (LANL 2011) and the removal of that effect by the cubic spline smoothers that were used by the ICRP and for this report.

The upper photon energy for the photon plots is 3 MeV. This energy was chosen because the MCNP6.1 tally used for estimating the benchmark DCCs was the “f6:p“ tally, which is a track length estimator of kerma rather than absorbed dose. The kerma and absorbed dose DCCs diverge at 3 MeV.

ATTACHMENT D
RESULTS OF REFERENCE CALCULATIONS (continued)

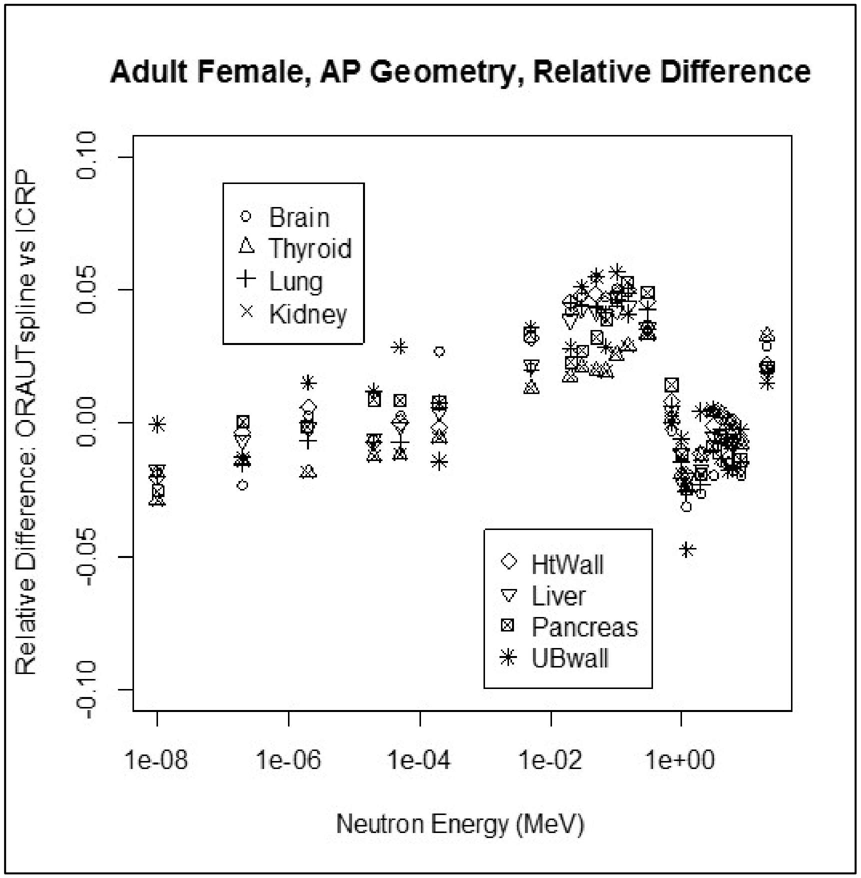

Figure D-1. Relative differences between ICRP-evaluated DCCs and ORAU Team-calculated DCCs, adult female reference organs, monoenergetic neutrons, AP geometry.

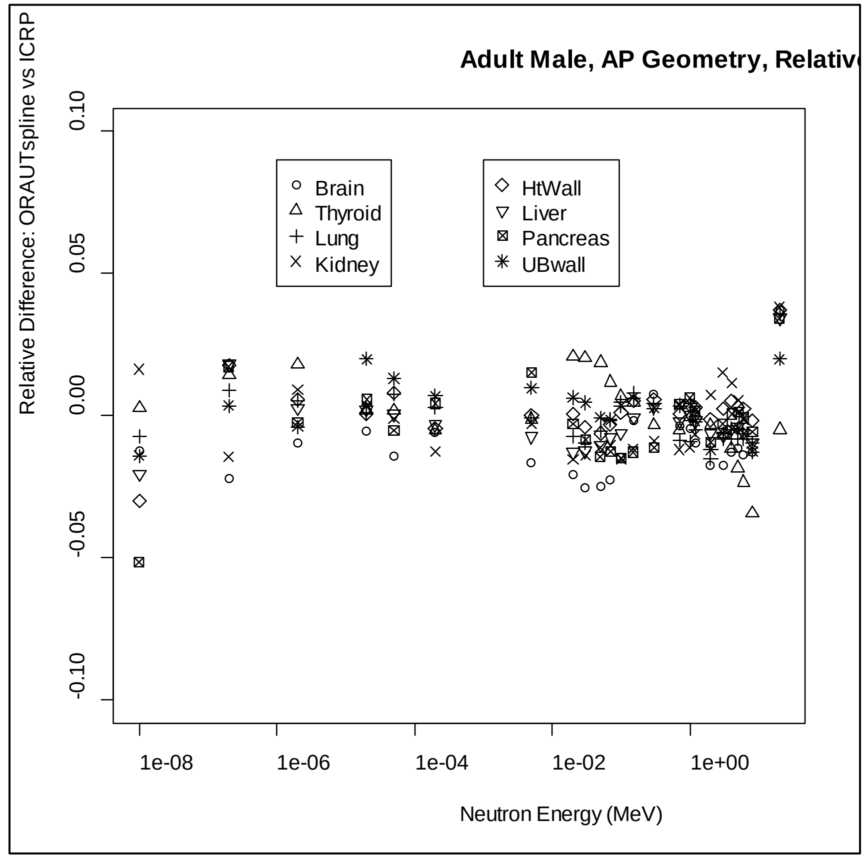

Figure D-2. Relative differences between ICRP-evaluated DCCs and ORAU Team-calculated DCCs, adult male reference organs, monoenergetic neutrons, AP geometry.

ATTACHMENT D
RESULTS OF REFERENCE CALCULATIONS (continued)

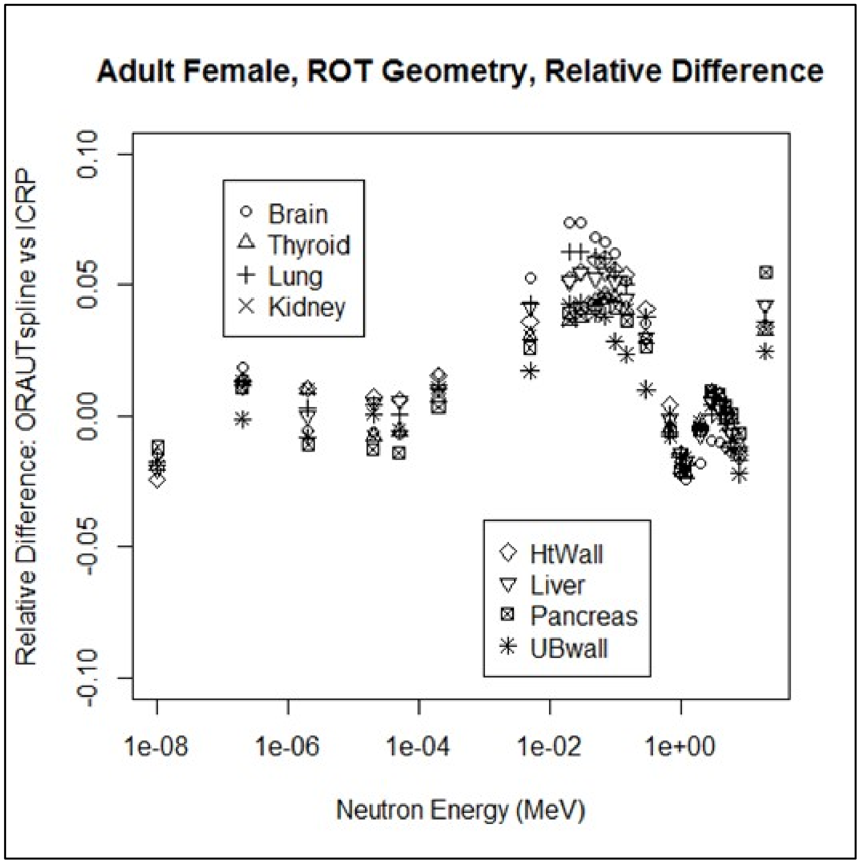

Figure D-3. Relative differences between ICRP-evaluated DCCsand ORAU Team-calculated DCCs, adult female reference organs, monoenergetic neutrons, ROT geometry.

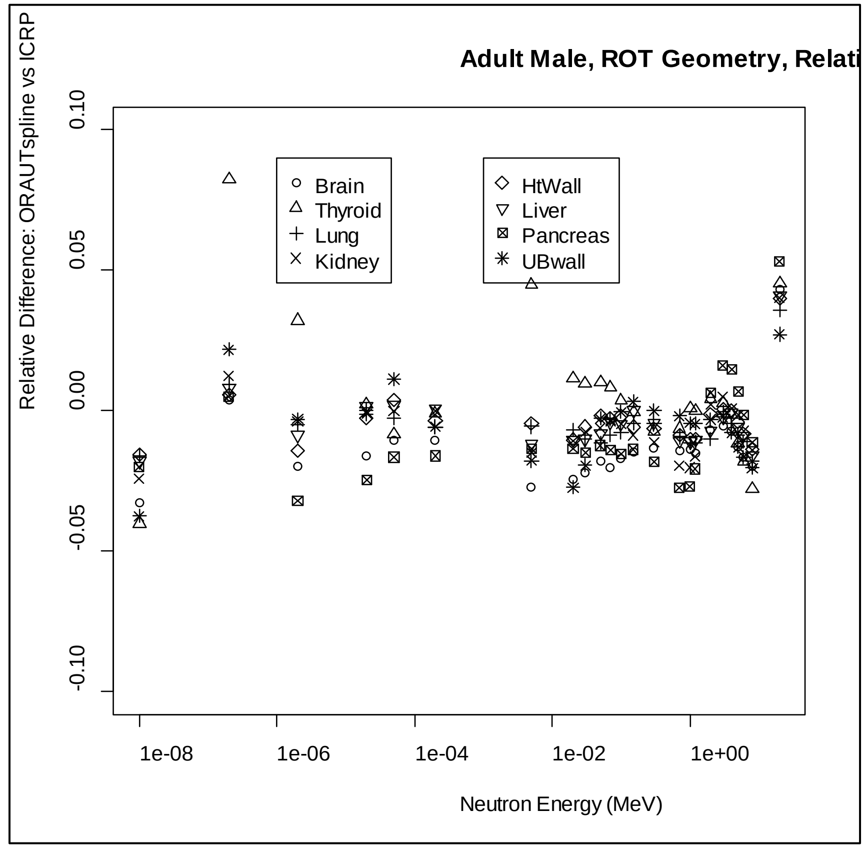

Figure D-4. Relative differences between ICRP-evaluated DCCs and ORAU Team-calculated DCCs, adult male reference organs, monoenergetic neutrons, ROT geometry.

ATTACHMENT D
RESULTS OF REFERENCE CALCULATIONS (continued)

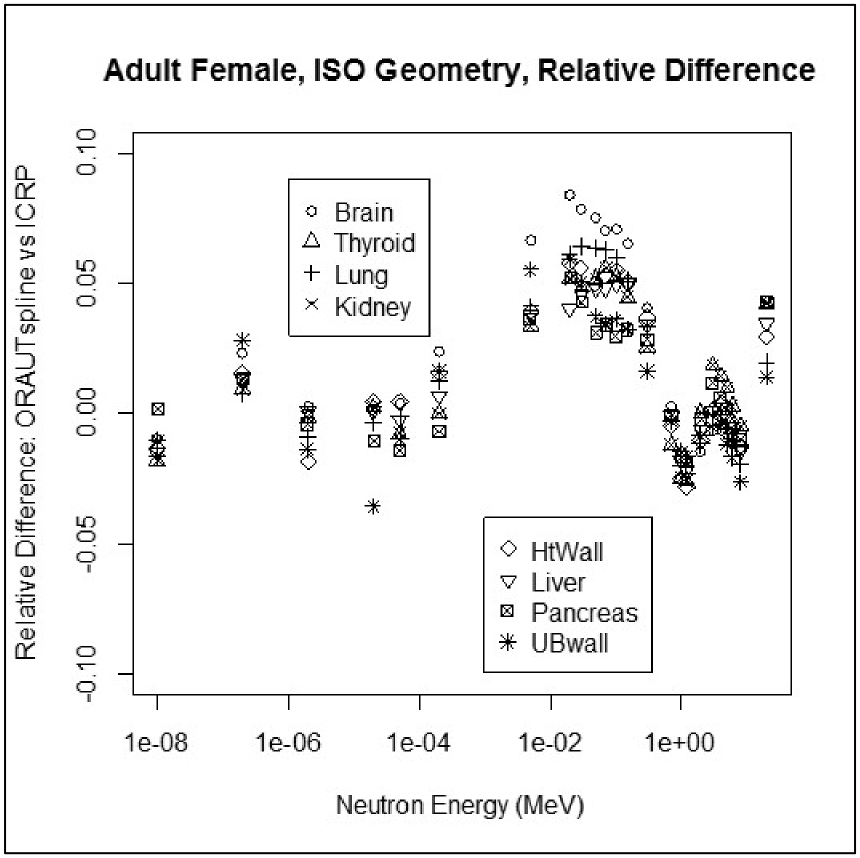

Figure D-5. Relative differences between ICRP-evaluated DCCs and ORAU Team-calculated DCCs, adult female reference organs, monoenergetic neutrons, ISO geometry.

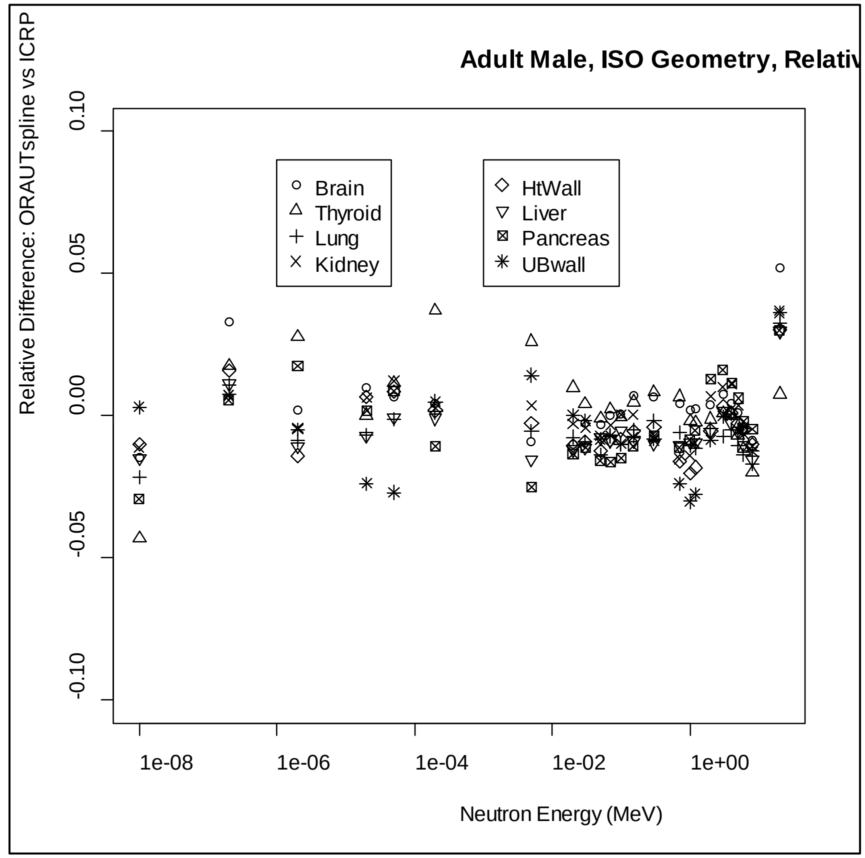

Figure D-6. Relative differences between ICRP-evaluated DCCs and ORAU Team-calculated DCCs, adult male reference organs, monoenergetic neutrons, ISO geometry.

ATTACHMENT D
RESULTS OF REFERENCE CALCULATIONS (continued)

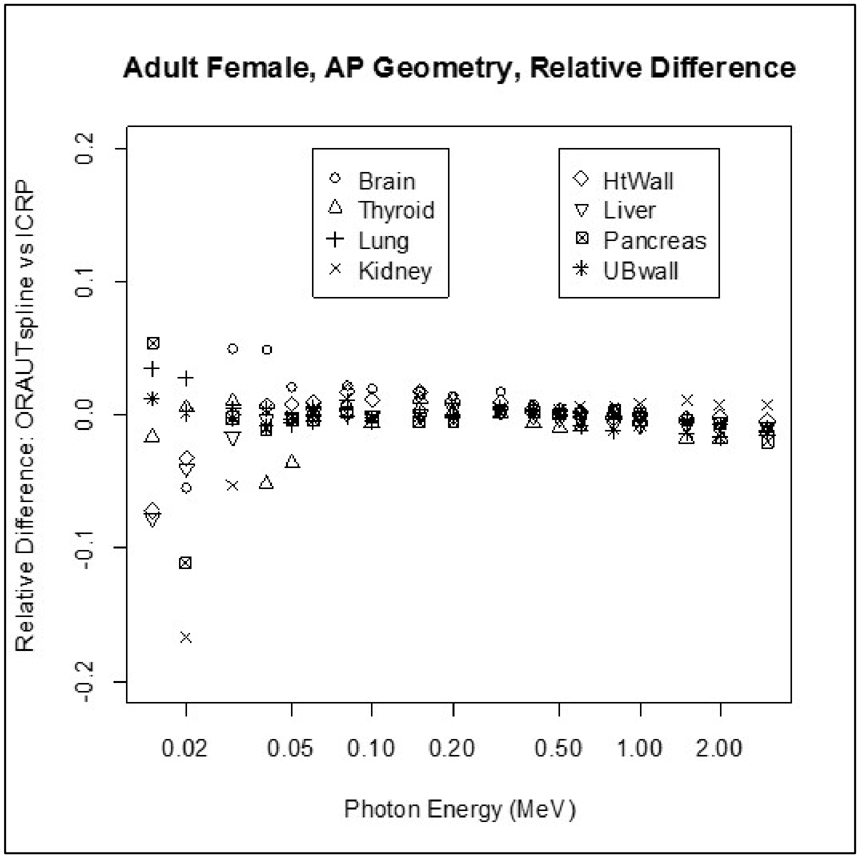

Figure D-7. Relative differences between ICRP-evaluated DCCs and ORAU Team-calculated DCCs, adult female reference organs, monoenergetic photons, AP geometry.

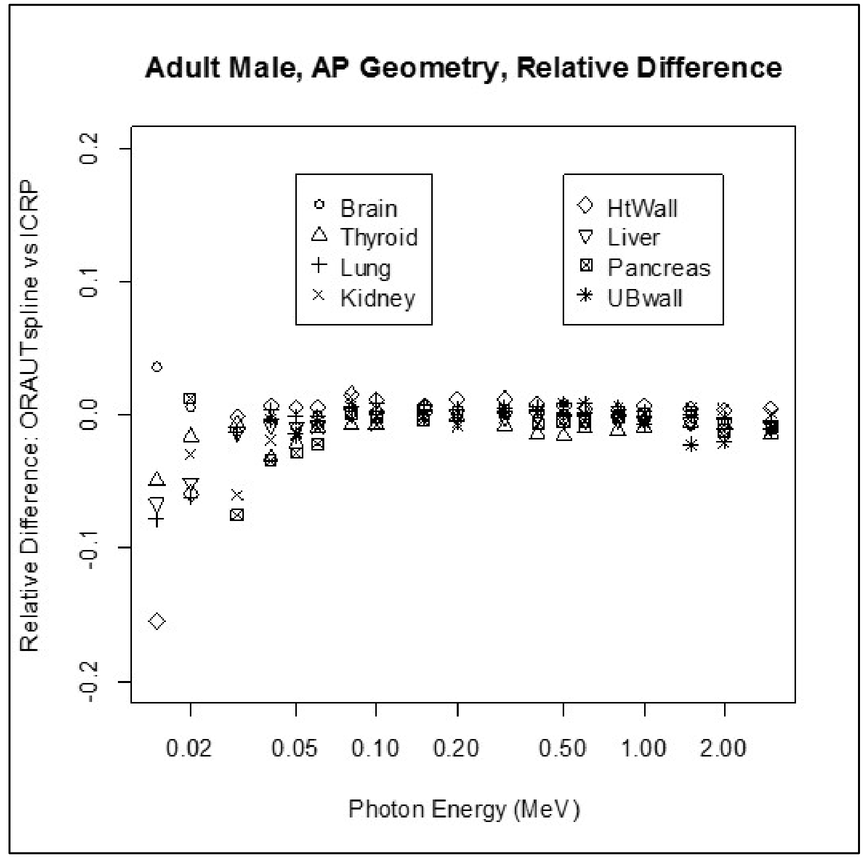

Figure D-8. Relative differences between ICRP-evaluated DCCs and ORAU Team-calculated DCCs, adult male reference organs, monoenergetic photons, AP geometry.

ATTACHMENT D
RESULTS OF REFERENCE CALCULATIONS (continued)

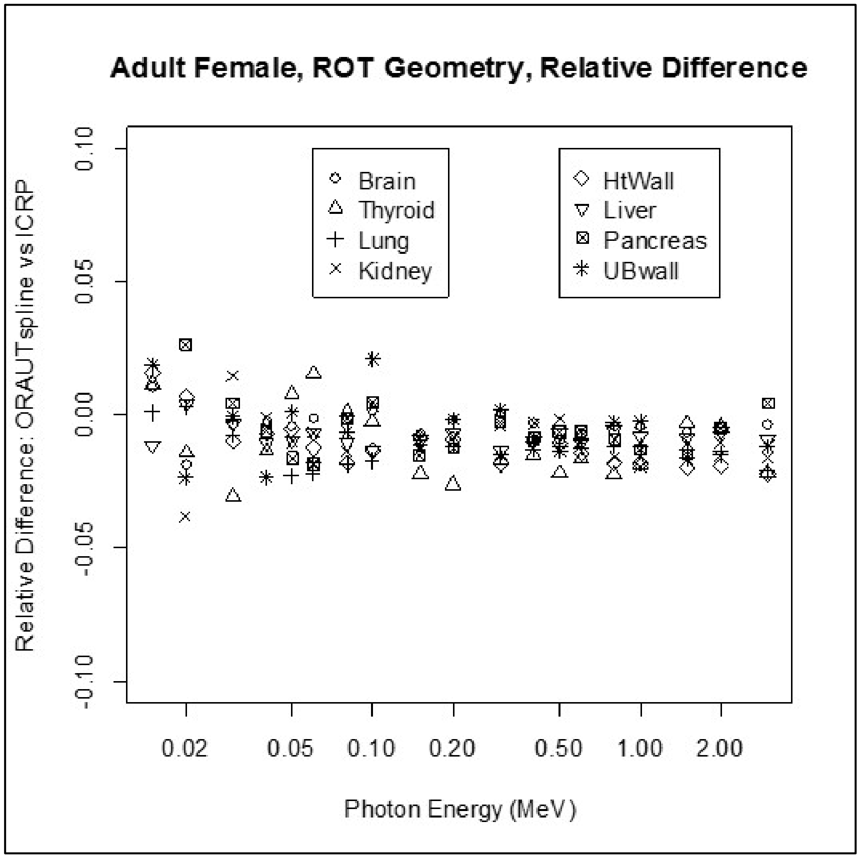

Figure D-9. Relative differences between ICRP-evaluated DCCs and ORAU Team-calculated DCCs, adult female reference organs, monoenergetic photons, ROT geometry.

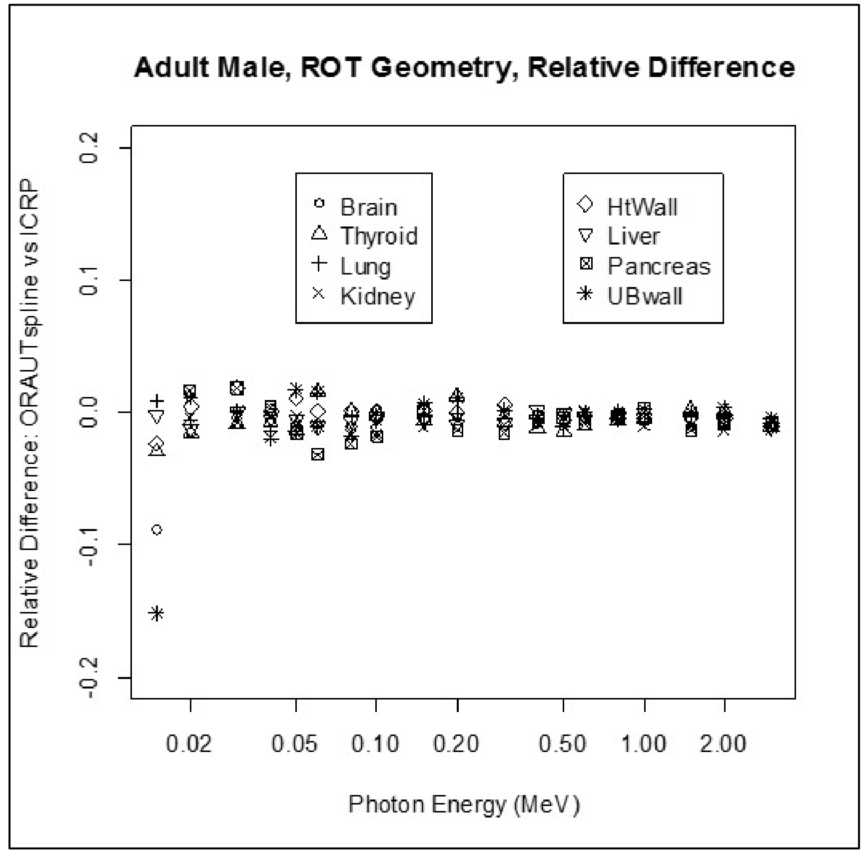

Figure D-10. Relative differences between ICRP-evaluated DCCs and ORAU Team-calculated DCCs, adult male reference organs, monoenergetic photons, ROT geometry.

ATTACHMENT D
RESULTS OF REFERENCE CALCULATIONS (continued)

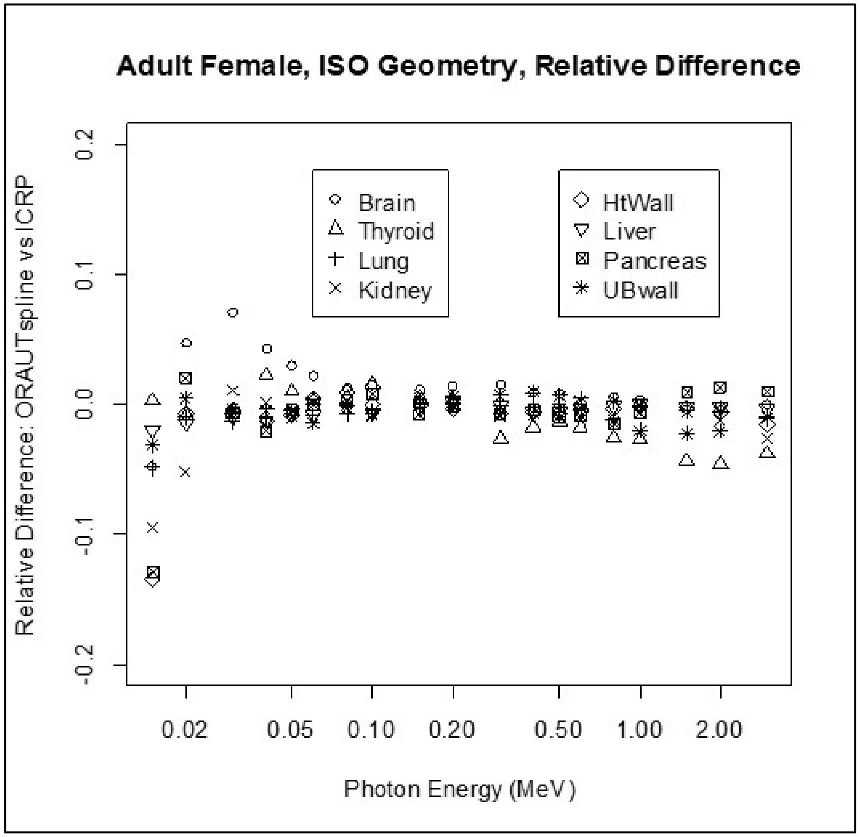

Figure D-11. Relative differences between ICRP-evaluated DCCs and ORAU Team-calculated DCCs, adult female reference organs, monoenergetic photons, ISO geometry.

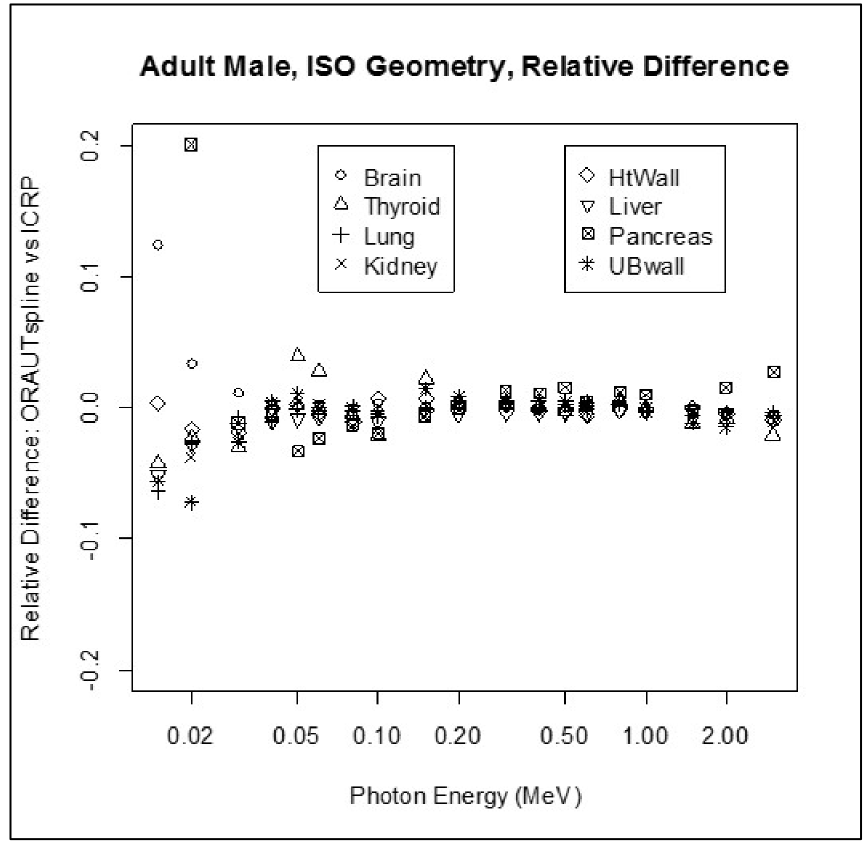

Figure D-12. Relative differences between ICRP-evaluated DCCs and ORAU Team-calculated DCCs, adult male reference organs, monoenergetic photons, ISO geometry.

ATTACHMENT D
RESULTS OF REFERENCE CALCULATIONS (continued)

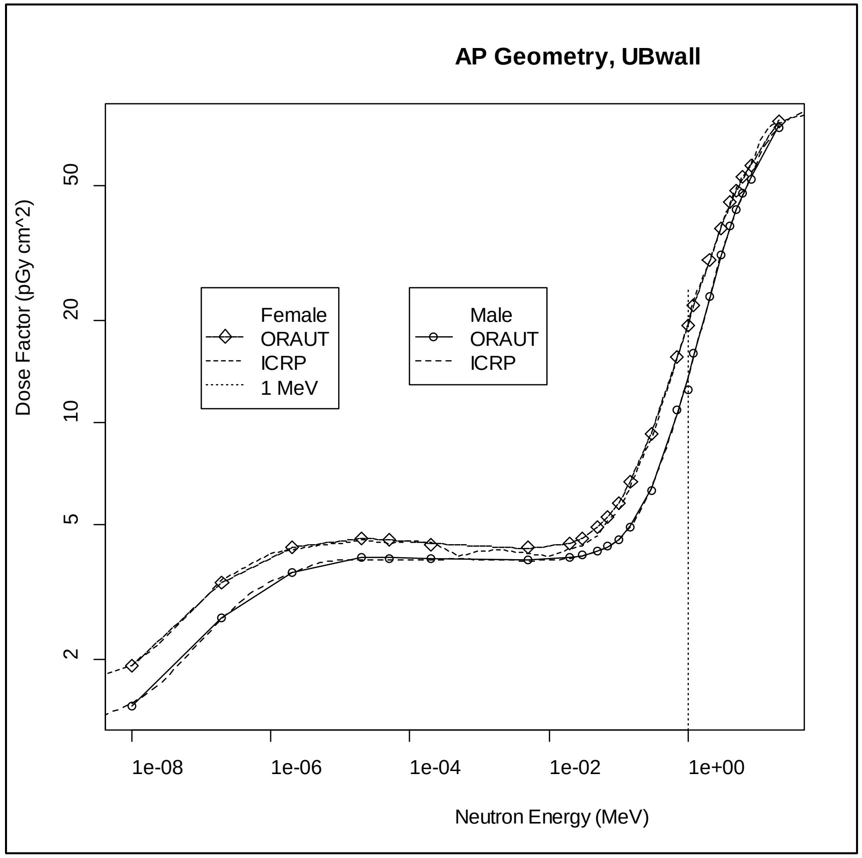

Figure D-13. Comparison between ICRP-evaluated DCCs and ORAU Team-calculated DCCs, adult female and male urinary bladder wall, monoenergetic neutrons, AP geometry.